

Kaon femtoscopy in Pb-Pb collisions at $\sqrt{s_{NN}} = 2.76$ TeV

(ALICE Collaboration) Acharya, S.; ...; Antičić, Tome; ...; Erhardt, Filip; ...; Gotovac, Sven; ...; Jerčić, Marko; ...; ...

Source / Izvornik: **Physical Review C, 2017, 96**

Journal article, Published version

Rad u časopisu, Objavljena verzija rada (izdavačev PDF)

<https://doi.org/10.1103/PhysRevC.96.064613>

Permanent link / Trajna poveznica: <https://urn.nsk.hr/urn:nbn:hr:217:367240>

Rights / Prava: [Attribution 4.0 International](#)/[Imenovanje 4.0 međunarodna](#)

Download date / Datum preuzimanja: **2025-02-20**



Repository / Repozitorij:

[Repository of the Faculty of Science - University of Zagreb](#)



Kaon femtoscopy in Pb-Pb collisions at $\sqrt{s_{NN}} = 2.76$ TeVS. Acharya *et al.**
(ALICE Collaboration)

(Received 1 October 2017; published 21 December 2017)

We present the results of three-dimensional femtoscopic analyses for charged and neutral kaons recorded by ALICE in Pb-Pb collisions at $\sqrt{s_{NN}} = 2.76$ TeV. Femtoscopy is used to measure the space-time characteristics of particle production from the effects of quantum statistics and final-state interactions in two-particle correlations. Kaon femtoscopy is an important supplement to that of pions because it allows one to distinguish between different model scenarios working equally well for pions. In particular, we compare the measured three-dimensional kaon radii with a purely hydrodynamical calculation and a model where the hydrodynamic phase is followed by a hadronic rescattering stage. The former predicts an approximate transverse mass (m_T) scaling of source radii obtained from pion and kaon correlations. This m_T scaling appears to be broken in our data, which indicates the importance of the hadronic rescattering phase at LHC energies. A k_T scaling of pion and kaon source radii is observed instead. The time of maximal emission of the system is estimated by using the three-dimensional femtoscopic analysis for kaons. The measured emission time is larger than that of pions. Our observation is well supported by the hydrokinetic model predictions.

DOI: [10.1103/PhysRevC.96.064613](https://doi.org/10.1103/PhysRevC.96.064613)**I. INTRODUCTION**

The extremely high energy densities achieved in heavy-ion collisions at the CERN Large Hadron Collider (LHC) are expected to lead to the formation of a quark-gluon plasma (QGP), a state characterized by partonic degrees of freedom [1,2]. The systematic study of many observables (transverse momentum spectra, elliptic flow, jets, femtoscopy correlations) measured at the Brookhaven National Laboratory Relativistic Heavy Ion Collider (RHIC) and at the LHC confirmed the presence of strong collective motion and the hydrodynamic behavior of the system (see, e.g., Refs. [3–9], respectively). Whereas hydrodynamics was used to describe momentum-based observables since quite a long time, it could not describe spatial distributions at decoupling. Correlation femtoscopy [commonly referred to as *femtoscopy* or *Hanbury–Brown–Twiss (HBT) interferometry*] measures the space-time characteristics of particle production by using particle correlations due to the effects of quantum statistics and strong and Coulomb final-state interactions [10–14]. The problem to describe the spatiotemporal scales derived from femtoscopy in heavy-ion collisions at RHIC was solved only a few years ago, strongly constraining the hydrodynamical models [15–17]. The following factors were understood to be important: existence of prethermal transverse flow, a crossover transition between quark-gluon and hadron matter, nonhydrodynamic behavior of the hadron gas at the latest stage (hadronic cascade phase), and correct matching between hydrodynamic and nonhydrodynamics phases (see, e.g., Ref. [15]).

New challenges for hydrodynamics appeared when data were obtained at the LHC: the large statistics now allows one to investigate not only pion femtoscopy, which is the most common femtoscopic analysis, but also femtoscopy of heavier particles in differential analyses with high precision.

The main objective of ALICE [18] at the LHC is to study the QGP. ALICE has excellent capabilities to study femtoscopy observables due to good track-by-track particle identification (PID), particle acceptance down to low transverse momenta p_T , and good resolution of secondary vertices. We already studied pion correlation radii in Pb-Pb collisions at 2.76 TeV [9,19]. Pion femtoscopy showed genuine effects originating from collective flow in heavy-ion collisions, manifesting as a decrease of the source radii with increasing pair transverse mass $m_T = (k_T^2 + m^2)^{1/2}$ [14,20], where $k_T = |\mathbf{p}_{T,1} + \mathbf{p}_{T,2}|/2$ is the average transverse momentum of the corresponding pair and m is the particles mass.

The next most numerous particle species after pions are kaons. The kaon analyses are expected to offer a cleaner signal compared with pions, because they are less affected by resonance decays. Studying charged and neutral kaon correlations together provides a convenient experimental consistency check, since they require different detection techniques. The theoretical models which describe pion femtoscopy well should describe kaon results with equal precision.

Of particular interest is the study of the m_T dependence of pion and kaon source radii. It was shown that the hydrodynamic picture of nuclear collisions for the particular case of small transverse flow leads to the same m_T behavior of the longitudinal radii (R_{long}) for pions and kaons [21]. This common m_T scaling for π and K is an indication that thermal freeze-out occurs simultaneously for π and K and that these two particle species are subject to the same velocity boost from collective flow. Previous kaon femtoscopy studies carried out in Pb-Pb collisions at the CERN Super Proton Synchrotron (SPS) by the NA44 and NA49 Collaborations [22,23] reported the decrease of R_{long} with m_T as $\sim m_T^{-0.5}$

*Full author list given at the end of the article.

Published by the American Physical Society under the terms of the [Creative Commons Attribution 4.0 International](https://creativecommons.org/licenses/by/4.0/) license. Further distribution of this work must maintain attribution to the author(s) and the published article's title, journal citation, and DOI.

as a consequence of the boost-invariant longitudinal flow. Subsequent studies carried out in Au-Au collisions at RHIC [24–27] have shown the same power in the m_T dependencies for π and K radii, consistent with a common freeze-out hypersurface. Like in the SPS data, no exact universal m_T scaling for the three-dimensional (3D) radii was observed at RHIC, but still these experiments observed an approximate m_T scaling for pions and kaons. The recent study of the m_T dependence of kaon three-dimensional radii performed by the PHENIX Collaboration [28] demonstrated breaking of this scaling especially for the “long” direction. PHENIX reported that the hydrokinetic model (HKM) describes well the overall trend of femtoscopic radii for pions and kaons [29,30].

We have published previously the study of one-dimensional correlation radii of different particle species: $\pi^\pm\pi^\pm$, $K^\pm K^\pm$, $K_S^0 K_S^0$, pp, and $p\bar{p}$ correlations in Pb-Pb collisions at $\sqrt{s_{NN}} = 2.76$ TeV for several intervals of centrality and transverse mass [31]. The decrease of the source radii with increasing transverse mass was observed for all types of particles, manifesting a fingerprint of collective flow in heavy-ion collisions. The one-dimensional femtoscopic radii demonstrated the approximate m_T scaling as was expected from hydrodynamic model considerations [14].

Recent calculations made within a (3 + 1)-dimensional [(3 + 1)-D] hydrodynamical model coupled with a statistical hadronization code taking into account the resonance contribution, THERMINATOR-2, showed the approximate scaling of the three-dimensional radii with transverse mass for pions, kaons, and protons [32]. An alternative calculation; that is, the hydrokinetic model, including a hydrodynamic phase as well as a hadronic rescattering stage, predicts the violation of such a scaling between pions and kaons at LHC energies [33]. Both models observe approximate scaling if there is no rescattering phase. It is suggested in Ref. [33] that rescattering has a significantly different influence on pions and kaons and is responsible for the violation of m_T scaling at the LHC energies. Moreover, the analysis of the emission times of pions and kaons obtained within HKM in Ref. [34] showed that kaons are emitted later than pions due to rescattering through the rather-long-lived $K^*(892)$ resonance. This effect can explain the m_T -scaling violation predicted in Ref. [33].

In Ref. [33] it was found that immediately decaying the $K^*(892)$ and $\phi(1020)$ resonances at the chemical freeze-out hypersurface has only a negligible influence on the kaon radii. In this scenario, resonances were allowed to be regenerated in the hadronic phase. Further analysis in Ref. [34] showed that it is indeed the regeneration of the $K^*(892)$ resonance through hadronic reactions which is responsible for the m_T -scaling violation predicted in Ref. [33]. This mechanism clearly manifests itself in the prolonged emission time of kaons caused by the rather long lifetime of the $K^*(892)$ resonance [33].

The approximate scaling of pion and kaon radii was predicted by investigating (3 + 1)-D hydrodynamical model + THERMINATOR-2 in Ref. [32] to hold for each of the three-dimensional radii separately. The scaling of one-dimensional pion and kaon radii was also studied in Ref. [32]. It was shown that, after averaging the three-dimensional radii and taking into account a mass-dependent Lorentz-boost factor, a deviation between one-dimensional pion and kaon radii appeared. These

circumstances made it impossible to discriminate between THERMINATOR-2 [32] and HKM calculations [33] in the earlier published one-dimensional analysis of pion and kaon radii by ALICE [31]. The three-dimensional study presented here is not impeded by these effects and allows one to discriminate between the hypothesis of approximate scaling of three-dimensional radii predicted in Ref. [32] and the strong scaling violation proposed in Ref. [33]. Thus the study of the m_T dependence of three-dimensional pion and kaon radii can unambiguously distinguish between the different freeze-out scenarios and clarify the existence of a significant hadronic phase.

One more interesting feature of femtoscopy studies of heavy-ion collisions concerns the ratio of radius components in the transverse plane. The strong hydrodynamic flow produces significant positive space-time correlations during the evolution of the freeze-out hypersurface. This influences the extracted radius parameters of the system in the plane perpendicular to the beam axis. The radius along the pair transverse momentum is reduced by the correlation with respect to the perpendicular one in the transverse plane. This effect appears to be stronger at LHC energies than at RHIC energies [35,36]. It was studied by the ALICE collaboration for pions in Pb-Pb collisions at 2.76 TeV [19] at different centralities. This work extends this study to kaons and compares the obtained transverse radii with those found in the analysis for pions and to the model calculations discussed above.

The paper is organized as follows: Section II explains the data selection and describes the identification of charged and neutral kaons. In Sec. III the details of the analysis of the correlation functions are discussed together with the investigation of the systematic uncertainties. Section IV presents the measured source radii as well as the extracted emission times and compares them to model predictions. Finally, Sec. V summarizes the results obtained and discusses them within the hydrokinetic approach.

II. DATA SELECTION

Large sets of data were recorded by the ALICE collaboration at $\sqrt{s_{NN}} = 2.76$ TeV in Pb-Pb collisions. The about 8 million events from 2010 (used only in the $K_S^0 K_S^0$ analysis) and about 40 million events from 2011 made it possible to perform the three-dimensional analyses of neutral and charged kaon correlations differentially in centrality and pair transverse momentum k_T . Three trigger types were used: minimum bias, semicentral (10%–50% collision centrality), and central (0%–10% collision centrality) [37]. The analyses were performed in the centrality ranges: (0%–5%), (0%–10%), (10%–30%), and (30%–50%). The centrality was determined by using the measured amplitudes in the V0 detector [37]. The following transverse momentum k_T bins were considered: (0.2–0.4), (0.4–0.6), and (0.6–0.8) GeV/c for charged kaons and (0.2–0.6), (0.6–0.8), (0.8–1.0), and (1.0–1.5) GeV/c for neutral kaons.

Charged particle tracking is generally performed by using the time projection chamber (TPC) [38] and the inner tracking

TABLE I. Single-particle selection criteria.

Charged kaon selection	
p_T	$0.15 < p_T < 1.5 \text{ GeV}/c$
$ \eta $	< 0.8
DCA _{transverse} to primary vertex	$< 2.4 \text{ cm}$
DCA _{longitudinal} to primary vertex	$< 3.0 \text{ cm}$
$N_{\sigma, \text{TPC}}$ (for $p < 0.5 \text{ GeV}/c$)	< 2
$N_{\sigma, \text{TPC}}$ (for $p > 0.5 \text{ GeV}/c$)	< 3
$N_{\sigma, \text{TOF}}$ (for $0.5 < p < 0.8 \text{ GeV}/c$)	< 2
$N_{\sigma, \text{TOF}}$ (for $0.8 < p < 1.0 \text{ GeV}/c$)	< 1.5
$N_{\sigma, \text{TOF}}$ (for $1.0 < p < 1.5 \text{ GeV}/c$)	< 1.0
Neutral kaon selection	
$ \eta $	< 0.8
Daughter-daughter DCA _{3D}	$< 0.3 \text{ cm}$
DCA _{3D} to primary vertex	$< 0.3 \text{ cm}$
Invariant mass	$0.480 < m_{\pi^+\pi^-} < 0.515 \text{ GeV}/c^2$
Daughter p_T	$> 0.15 \text{ GeV}/c$
Daughter $ \eta $	< 0.8
Daughter DCA _{3D} to primary vertex	$> 0.4 \text{ cm}$
Daughter $N_{\sigma, \text{TPC}}$	< 3
Daughter $N_{\sigma, \text{TOF}}$ (for $p > 0.8 \text{ GeV}/c$)	< 3

system (ITS) [18]. The ITS also provides high spatial resolution in determining the primary collision vertex.

Particle identification (PID) for reconstructed tracks was carried out by using both the TPC and the time-of-flight (TOF) detector [39]. For TPC PID, a parametrization of the Bethe-Bloch formula was employed to calculate the specific energy loss (dE/dx) in the detector expected for a particle with a given mass and momentum. For PID with TOF, the particle mass hypothesis was used to calculate the expected time of flight as a function of track length and momentum. For each PID method, a value N_σ was assigned to each track denoting the number of standard deviations between the measured track dE/dx or time of flight and the calculated one as described above. Different cut values of N_σ were chosen based on detector performance for various particle types and track momenta (see Table I for specific values used in both analyses). More details on PID can be found in Secs. 7.2–7.5 of Ref. [40].

The analysis details for charged and neutral kaons are discussed separately below. All major selection criteria are also listed in Table I.

A. Charged kaon selection

Track reconstruction for the charged kaon analysis was performed by using the tracks' signal in the TPC. The TPC is divided by the central electrode into two halves, each of them composed of 18 sectors (covering the full azimuthal angle) with 159 padrows placed radially in each sector. A track signal in the TPC consists of space points (clusters), each of which is reconstructed in one of the padrows. A track was required to be composed out of at least 70 such clusters. The parameters of the track are determined by performing a Kalman fit to a set of clusters with an additional constraint that the track passes through the primary vertex. The quality of the fit is requested to have χ^2/NDF better than two. The transverse momentum of each track was determined from its curvature in

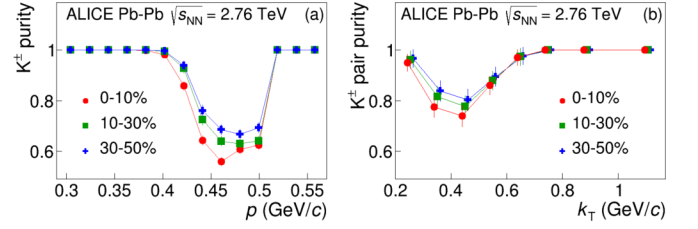


FIG. 1. (a) Single K^\pm purity and (b) pair purity for small relative momenta for different centralities. In panel (b), the k_T values for different centrality intervals are slightly offset for clarity.

the uniform magnetic field. The momentum from this fit in the TPC was used in the analysis. Tracks were selected based on their distance of closest approach (DCA) to the primary vertex, which was required to be less than 2.4 cm in the transverse direction and less than 3.0 cm in the longitudinal direction.

K^\pm identification was performed by using the TPC (for all momenta) and the TOF detector (for $p > 0.5 \text{ GeV}/c$). The use of different values for $N_{\sigma, \text{TPC}}$ and $N_{\sigma, \text{TOF}}$ was the result of studies to obtain the best kaon purity, which is defined as the fraction of accepted kaon tracks that corresponds to true kaon particles, while retaining a decent efficiency. The estimation of purity for $p < 0.5 \text{ GeV}/c$ was performed by parametrizing the TPC dE/dx distribution in momentum slices for the contributing species [40]. The dominant contamination for charged kaons comes from e^\pm in the momentum range $0.4 < p < 0.5 \text{ GeV}/c$. The purity for $p > 0.5 \text{ GeV}/c$, where the TOF information was employed, was studied with HIJING [41] simulations using GEANT [42] to model particle transport through the detector; the charged kaon purity was estimated to be greater than 99%. The momentum dependence of the single kaon purity is shown in Fig. 1(a). The pair purity is calculated as the product of two single-particle purities, where the momenta are taken from the experimentally determined distribution. The K^\pm pair purity as a function of k_T at three different centralities is shown in Fig. 1(b). Kaon pair transverse momentum is an averaged p_T of single kaons taken from the whole p_T range, which is the reason why the pair purities are larger than single-particle purities.

Two kinds of two-track effects have been investigated: splitting, where a signal produced by one particle is incorrectly reconstructed as two tracks, and merging, where two particles are reconstructed as only one track. These detector inefficiencies can be suppressed by employing specific pair selection criteria. We used the same procedure as in Ref. [19] which works here as well with slightly modified cut values. Charged kaon pairs were required to have a separation of $|\Delta\varphi^*| > 0.04$ and $|\Delta\eta| > 0.02$. Here, φ^* is the azimuthal position of the track in the TPC at $R = 1.2 \text{ m}$, taking into account track curvature in the magnetic field, and η is the pseudorapidity. Also, all track pairs sharing more than 5% of TPC clusters were rejected.

B. Neutral kaon selection

The decay channel $K_S^0 \rightarrow \pi^+\pi^-$ was used for the identification of neutral kaons. The secondary pion tracks were reconstructed by using TPC and ITS information. The single-particle cuts for parents (K_S^0) and daughters (π^\pm) used in

the decay-vertex reconstruction are shown in Table I. The daughter-daughter DCA; that is, the distance of closest approach of the two daughter pions from a candidate K_S^0 decay, proved useful in rejecting background topologies. PID for the pion daughters was performed by using both TPC (for all momenta) and TOF (for $p > 0.8 \text{ GeV}/c$). The very good detector performance is reflected in the full width at half maximum (FWHM) of the K_S^0 peak of only $8 \text{ MeV}/c^2$. The selection criteria used in this analysis were chosen as a compromise to maximize statistics while keeping a high signal purity. The neutral kaon purity [defined as $\text{Sig.}/(\text{Sig.} + \text{Bkg.})$ for $0.480 < m_{\pi^+\pi^-} < 0.515 \text{ GeV}/c^2$] was larger than 0.95.

Two main two-particle cuts were used in the neutral kaon analysis. To resolve two-track inefficiencies associated with the daughter tracks, such as the splitting or merging of tracks discussed above, a separation cut was employed in the following way: For each kaon pair, the spatial separation between the same-sign pion daughters was calculated at several points throughout the TPC (every 20 cm radially from 85 to 245 cm) and averaged. If the average separation of either pair of tracks was below 5 cm, the kaon pair was not used. Another cut was used to prevent two reconstructed kaons from using the same daughter track. If two kaons shared a daughter track, one of them was excluded by using a procedure which compared the two K_S^0 candidates and kept the candidate whose reconstructed parameters best matched those expected for a true K_S^0 particle in two of three categories (smaller K_S^0 DCA to primary vertex, smaller daughter-daughter DCA, and K_S^0 mass closer to the Particle Data Group value [43]). This procedure was shown, using HIJING + GEANT simulations, to have a success rate of about 95% in selecting a true K_S^0 particle over a fake one. More details about the $K_S^0 K_S^0$ analysis can be found in Refs. [44,45]. K_S^0 candidate selection criteria developed in other works [31] were used here as well; they are included in Table I.

III. CORRELATION FUNCTIONS

The femtoscopic correlation function C is constructed experimentally as the ratio $C(\mathbf{q}) = A(\mathbf{q})/B(\mathbf{q})$, where $A(\mathbf{q})$ is the measured distribution of the difference $\mathbf{q} = \mathbf{p}_2 - \mathbf{p}_1$ between the three-momenta of the two particles \mathbf{p}_1 and \mathbf{p}_2 taken from the same event, $B(\mathbf{q})$ is a reference distribution of pairs of particles taken from different events (mixed). For a detailed description of the formalism, see, e.g., Ref. [13]. The pairs in the denominator distribution $B(\mathbf{q})$ are constructed by taking a particle from one event and pairing it with a particle from another event with a similar centrality and primary vertex position along the beam direction. Each event is mixed with five (ten) others for the K_S^0 (K^\pm) analysis. The numerator and denominator are normalized in the full $q = (|\mathbf{q}|^2 - q_0^2)^{1/2}$ range used ($0-0.3 \text{ GeV}/c$) such that $C(q) \rightarrow 1$ means no correlation. Pair cuts have been applied in exactly the same way for the same-event (signal) and mixed-event (background) pairs.

The momentum difference is calculated in the longitudinally comoving system (LCMS), where the longitudinal pair momentum vanishes, and is decomposed into $(q_{\text{out}}, q_{\text{side}}, q_{\text{long}})$, with the “long” axis going along the beam, “out” along the pair transverse momentum, and “side” perpendicular to the latter in the transverse plane (Bertsch–Pratt convention).

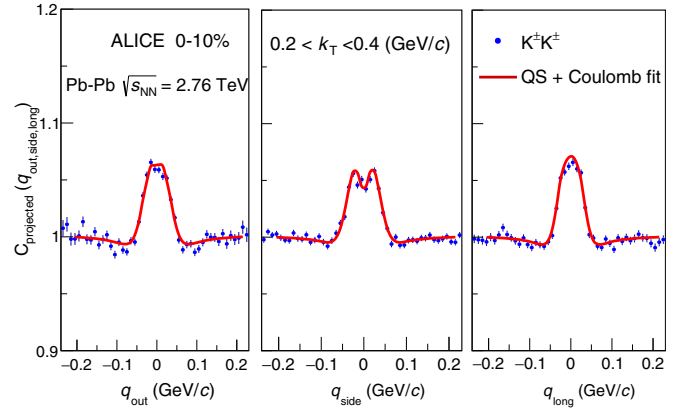


FIG. 2. A sample projected $K^\pm K^\pm$ correlation function with fit. The error bars are statistical only. Systematic uncertainties on the points are equal to or less than the statistical error bars shown.

The correlation functions have been corrected for momentum resolution effects, by using the HIJING event generator and assigning a quantum-statistical weight to each particle pair. Furthermore, these modified events were propagated through the full simulation of the ALICE detectors [18]. The ratios of the correlation functions obtained before and after this full event simulation have been taken as the correction factors. The correlation function from the data has been divided by this q -dependent factor. The correction increases the obtained radii by 3%–5%.

A. Charged kaon

The three-dimensional correlation functions were fit by the Bowler–Sinyukov formula [46,47]:

$$C(\mathbf{q}) = N(1 - \lambda) + N\lambda K(q) \left[1 + \exp(-R_{\text{out}}^2 q_{\text{out}}^2 - R_{\text{side}}^2 q_{\text{side}}^2 - R_{\text{long}}^2 q_{\text{long}}^2) \right], \quad (1)$$

where R_{out} , R_{side} , and R_{long} are the Gaussian femtoscopic radii in the LCMS frame, N is the normalization factor, and q is the momentum difference in the pair rest frame (PRF).¹ The λ parameter, which characterizes the correlation strength, can be affected by long-lived resonances, coherent sources [48–50], and non-Gaussian features of the particle-emission distribution. We account for Coulomb effects through $K(q)$, calculated according to Refs. [47,49] as

$$K(q) = C(\text{QS} + \text{Coulomb})/C(\text{QS}). \quad (2)$$

Here, the theoretical correlation function $C(\text{QS})$ takes into account quantum statistics only and $C(\text{QS} + \text{Coulomb})$ considers quantum statistics and the Coulomb final-state interaction (FSI) contribution to the wave function [13].

The experimental correlation functions have been corrected for purity according to

$$C_{\text{corrected}} = (C_{\text{raw}} - 1 + \zeta)/\zeta, \quad (3)$$

¹ Average q in PRF for the given “out-side-long” bin is determined during the $C(\mathbf{q})$ construction and used as an argument of the K function.

TABLE II. The f_0 and a_0 masses and coupling parameters, all in GeV.

Ref.	m_{f_0}	$\gamma_{f_0\text{KK}}$	$\gamma_{f_0\pi\pi}$	m_{a_0}	$\gamma_{a_0\text{KK}}$	$\gamma_{a_0\pi\eta}$
[52]	0.973	2.763	0.5283	0.985	0.4038	0.3711
[53]	0.996	1.305	0.2684	0.992	0.5555	0.4401
[54]	0.996	1.305	0.2684	1.003	0.8365	0.4580
[55]	0.978	0.792	0.1990	0.974	0.3330	0.2220

where ζ is the pair purity taken from Fig. 1.

Figure 2 shows a sample projected $K^\pm K^\pm$ correlation function with a fit performed according to Eq. (1). When the 3D correlation function is projected onto one axis, the momentum differences in the two other directions are required to be within $(-0.04, 0.04)$ GeV/ c .

B. Neutral kaon

$K_S^0 K_S^0$ correlation functions were fit by using a parametrization which includes Bose–Einstein statistics as well as strong final-state interactions [26,51]. Strong final-state interactions have an important effect on $K_S^0 K_S^0$ correlations. Particularly, the $K^0 \bar{K}^0$ channel is affected by the near-threshold resonances $f_0(980)$ and $a_0(980)$. Using the equal emission time approximation in the pair rest frame (PRF) [51], the elastic $K^0 \bar{K}^0$ transition is written as a stationary solution $\Psi_{-\vec{k}^*}(\vec{r}^*)$ of the scattering problem in the PRF, where \vec{k}^* and \vec{r}^* represent the momentum of a particle and the emission separation of the pair in the PRF (the $-\vec{k}^*$ subscript refers to a reversal of time from the emission process), which at large distances has the asymptotic form of a superposition of a plane wave and an outgoing spherical wave,

$$\Psi_{-\vec{k}^*}(\vec{r}^*) = e^{-i\vec{k}^* \cdot \vec{r}^*} + g(k^*) \frac{e^{ik^* r^*}}{r^*}, \quad (4)$$

where $g(k^*)$ is the s -wave scattering amplitude for a given system. For $K^0 \bar{K}^0$, $g(k^*)$ is dominated by the f_0 and a_0 resonances and written in terms of the resonance masses and decay couplings [26]:

$$g(k^*) = \frac{1}{2} [g_0(k^*) + g_1(k^*)], \quad (5)$$

$$g_I(k^*) = \frac{\gamma_r}{m_r^2 - s - i\gamma_r k^* - i\gamma_r' k_r'}. \quad (6)$$

Here, $s = 4(m_K^2 + k^{*2})$; $\gamma_r(\gamma_r')$ refers to the couplings of the resonances to the $f_0 \rightarrow K^0 \bar{K}^0$ ($f_0 \rightarrow \pi\pi$) and $a_0 \rightarrow K^0 \bar{K}^0$ ($a_0 \rightarrow \pi\eta$) channels; m_r is the resonance mass; and k_r' refers to the momentum in the PRF of the second decay channel ($f_0 \rightarrow \pi\pi$ or $a_0 \rightarrow \pi\eta$) with the corresponding partial width $\Gamma_r' = \gamma_r' k_r' / m_r$. The amplitudes g_I of isospin $I = 0$ and $I = 1$ refer to the f_0 and a_0 , respectively. The parameters associated with the resonances and their decays are taken from several experiments [52–55], and the values are listed in Table II.

The correlation function is then calculated by integrating $\Psi_{-\vec{k}^*}(\vec{r}^*)$ in the Koonin–Pratt equation [56,57]

$$C(\vec{k}^*, \vec{K}) = \int d^3\vec{r}^* S_{\vec{K}}(\vec{r}^*) |\Psi_{-\vec{k}^*}^S(\vec{r}^*)|^2, \quad (7)$$

where $S_{\vec{K}}(\vec{r}^*)$ is the Gaussian source distribution in terms of R_{out} , R_{side} , and R_{long} , \vec{K} is the average pair momentum, and $\Psi_{-\vec{k}^*}^S(\vec{r}^*)$ is the symmetrized version of $\Psi_{-\vec{k}^*}(\vec{r}^*)$ for bosons. Although Eq. (7) can be integrated analytically for $K_S^0 K_S^0$ correlations with FSI for the one-dimensional case [26], for the three-dimensional case this integration cannot be performed analytically. To form the 3D correlation function, we combine a Monte Carlo emission simulation with a calculation of the two-particle wave function, thus performing a numerical integration of Eq. (7). The Monte Carlo (MC) emission simulation consists of generating the pair positions sampled from a three-dimensional Gaussian in the PRF, with three input radii as the width parameters, and generating the particle momenta sampled from a distribution taken from data. Using the MC-sampled positions and momenta, we calculate $\Psi_{-\vec{k}^*}^S(\vec{r}^*)$. We then build a correlation function by using the wave function weights to form the signal distribution, and an unweighted distribution acts as a background. This theoretical correlation function is then used to fit the data. Finally, we make a Lorentz boost, γ , of R_{out} from the PRF to the LCMS frame (R_{side} and R_{long} are not affected by the boost). More details on the 3D fitting procedure can be found in Ref. [44].

Figure 3 shows a sample projected $K_S^0 K_S^0$ correlation function with fit. Also shown is the contribution to the fit from the quantum statistics part only. As seen, the FSI part produces a significant depletion of the correlation function in the q range 0–0.1 GeV/ c in each case.

C. Systematic uncertainties

The effects of various sources of systematic uncertainty on the extracted fit parameters were studied as functions of centrality and k_T . For each source, we take the maximal deviation and apply it symmetrically as the uncertainty. Table III shows minimum and maximum uncertainty values for various sources of systematic uncertainty for charged and neutral kaons. The systematic errors are summed up quadratically. The values of the total uncertainty are not necessarily equal to the sum of the individual uncertainties, because the latter can come from different centrality or k_T bins. Both analyses studied the effects of changing the selection criteria used for the events, particles, and pairs (variation of cut values up to $\pm 25\%$) and varying the range of q values over which the fit is performed (variation of q limits up to $\pm 25\%$). Uncertainties associated with momentum resolution corrections are included into the K^\pm analysis; for the K_S^0 analysis, these uncertainties are found to be small compared with other contributions. Both analyses were performed separately for the two different polarities of the ALICE solenoid magnetic field, and the difference was found to be negligible.

For the K_S^0 fitting procedure, the mean γ value is calculated for each centrality and k_T selection and used to scale R_{out} . However, each bin has a spread of γ values associated with it. The standard deviation of the mean γ value for each k_T bin was used as an additional source of systematic error for R_{out} . For K_S^0 , an uncertainty on the strong FSI comes from the fact that several sets of $f_0(980)$ and $a_0(980)$ parameters are available

TABLE III. Minimum and maximum uncertainty values for various sources of systematic uncertainty for charged and neutral kaons (in percent). Note that each value is the maximum uncertainty from a specific source but can pertain to a different centrality or k_T bin. Thus, the maximum total uncertainties are smaller than (or equal to) the quadratic sum of the maximum individual uncertainties.

	R_{out} [%]	R_{side} [%]	R_{long} [%]	λ [%]
Charged kaon				
Single-particle selection	0–2	0–2	0–2	0–2
PID and purity	<0.1	<0.1	<0.1	1–10
Pair selection	2–8	1–6	2–10	6–15
Fit range	1–3	1–4	1–7	1–7
Coulomb function	3–5	1–2	2–3	8–10
Momentum resolution	1–2	1–2	1–3	2–6
Total (quad. sum)	7–11	7–9	7–12	10–17
Neutral kaon				
Single-particle and pair selection	0–1	1–5	1–4	6–14
Pair selection	2–8	1–6	2–10	6–15
FSI Model	1–6	1–6	1–15	3–9
γ	5–10	<0.1	<0.1	<0.1
Fit range	0–6	0–6	0–10	0–6
Momentum resolution	<0.1	0–3	0–6	2–3
Total (quad. sum)	6–11	3–7	2–15	7–16

[52–55]; each set is used to fit the data, the results are averaged, and the maximal difference was taken as a systematic error.

The K^\pm analysis has uncertainties associated with the choice of the radius for the Coulomb function. For each correlation function it is set to the value from the one-dimensional analysis [31]. Its variation by ± 1 fm is a source of systematic uncertainty. Another source of systematic uncertainty is misidentification of particles and the associated purity correction. A 10% variation of the parameters in the purity correction was performed. We also incorporated sets with a reduced electron contamination by (i) tightening the PID criteria, in particular extending the momentum range where the TOF signal was used and requiring the energy-loss measurement to be consistent with the kaon hypothesis within one sigma, and (ii) completely excluding the momentum range 0.4–0.5 GeV/c.

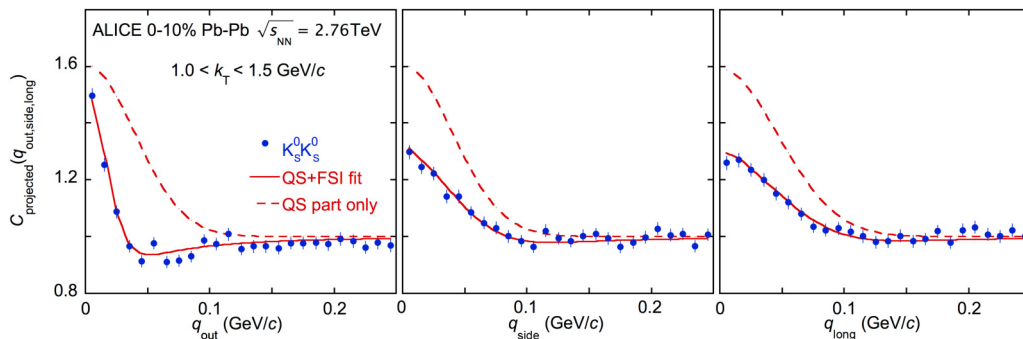


FIG. 3. A sample projected $K_S^0 K_S^0$ correlation function with fit. Also shown is the contribution to the fit from the quantum statistics part only. The error bars are statistical only. Systematic uncertainties on the points are equal to or less than the statistical error bars shown.

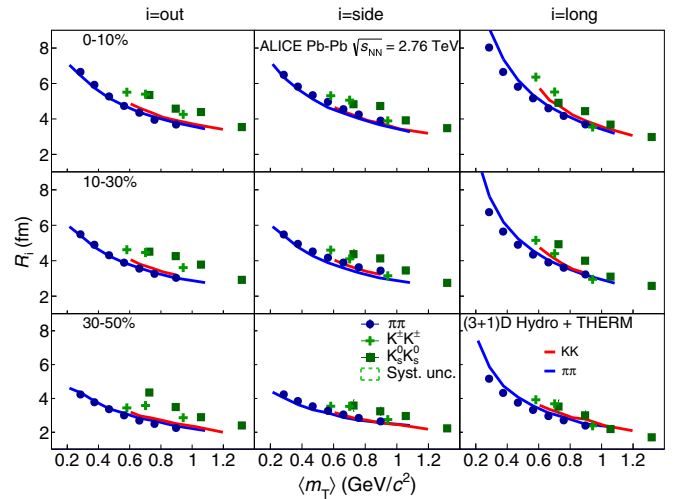


FIG. 4. The 3D LCMS radii vs m_T for charged (light green crosses) and neutral (dark green squares) kaons and pions [19] (blue circles) in comparison with the theoretical predictions of the (3 + 1)-D Hydro + THERMINATOR-2 model [32] for pions (blue solid lines) and kaons (red solid lines).

IV. RESULTS AND DISCUSSION

Figure 4 shows the m_T dependence of the extracted femtoscopic radii R_{out} , R_{side} , and R_{long} in three centrality selections for pions [19] and charged and neutral kaons. The obtained radii are smaller for more peripheral collisions than for central ones. The radii decrease with increasing m_T and each particle species roughly follows an $m_T^{-1/2}$ dependence. The radii in “out” and “long” directions exhibit larger values for kaons than for pions at the same transverse mass demonstrating that the m_T scaling is broken. This difference increases with centrality and is maximal for the most-central collisions. Also presented in Fig. 4 are the predictions of the (3 + 1)-D hydrodynamical model coupled with the statistical hadronization code THERMINATOR-2 [32]. The model describes well the m_T dependence of pion radii, but underestimates kaon radii. Consistent with the data, the (3 + 1)-D Hydro + THERMINATOR-2 model shows mild breaking in the “long” direction for central collisions, but it underestimates the breaking in the “out” direction. The

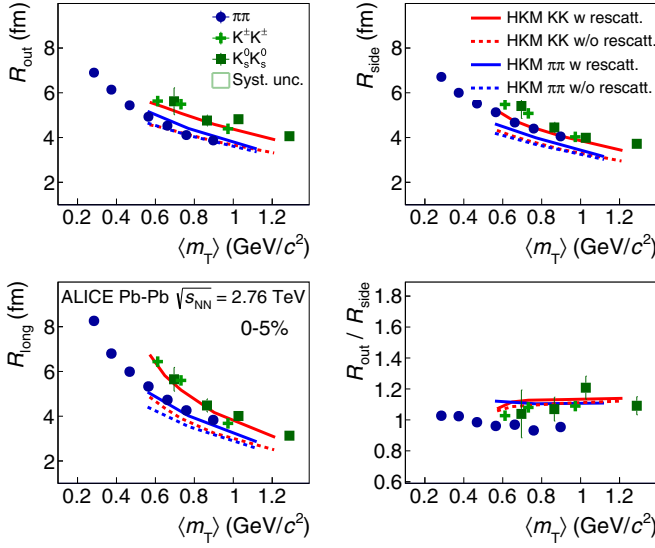


FIG. 5. The 3D LCMS radii vs m_T for 0%–5% most-central collisions in comparison with the theoretical predictions of HKM [33] for pions (blue lines) and kaons (red lines).

significance of this breaking of the scaling is discussed further in this section.

In addition to the aforementioned three-dimensional radii, here for the 0%–5% most-central events, Fig. 5 also shows the m_T dependence of the ratio $R_{\text{out}}/R_{\text{side}}$ for charged and neutral kaons in comparison with HKM predictions [33] with and without the hadronic rescattering phase. The HKM calculations without rescattering exhibit an approximate m_T scaling but do not describe the data, while the data are well reproduced by the full hydrokinetic model calculations thereby showing the importance of the rescattering phase at LHC energies. The R_{out} and R_{side} radii are both influenced by flow and rescatterings, so their ratio is rather robust against these effects. The fact that $R_{\text{out}}/R_{\text{side}}$ ratio of pions and kaons

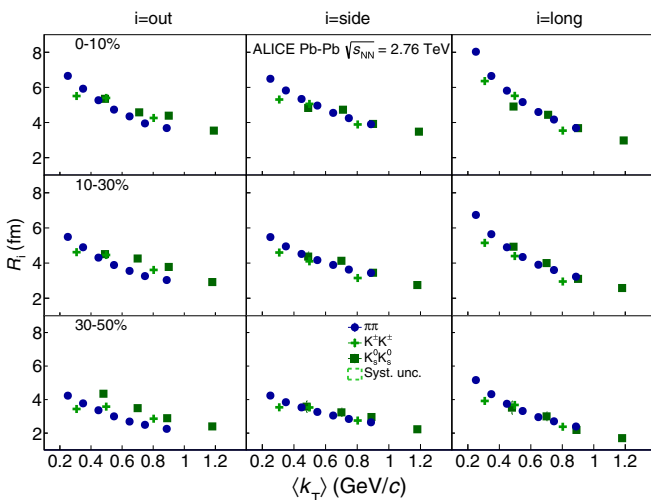


FIG. 6. The 3D LCMS radii vs k_T for charged (light green crosses) and neutral (dark green squares) kaons and pions [19] (blue circles).

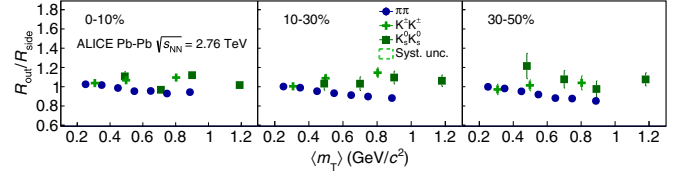


FIG. 7. $R_{\text{out}}/R_{\text{side}}$ vs m_T for pions [19] and kaons for different centrality intervals.

coincide in the HKM simulations (Fig. 5) is related to some underestimation of R_{side} radii for pions while pion R_{out} radii are slightly overestimated in the model.

It was predicted in Ref. [33] that the radii scale better with k_T at LHC energies as a result of the interplay of different factors in the model, including the particular initial conditions. Figure 6 illustrates the k_T dependence of the femtoscopic radii R_{out} , R_{side} , and R_{long} . Unlike the m_T dependence, the radii seem to scale better with k_T in accordance with this prediction.

The ratio $R_{\text{out}}/R_{\text{side}}$ appears to be sensitive to the space-time correlations present at the freeze-out hypersurface [19,35,36]. As it was observed in Ref. [19], the ratio for pions is consistent with unity, slowly decreasing for more peripheral collisions and higher k_T . In Fig. 7, the ratio $R_{\text{out}}/R_{\text{side}}$ is shown for pions and kaons at different centralities. The systematic uncertainties partially cancel in the ratio. Systematic uncertainties are correlated in m_T for each type of particle pair; no correlation between the systematic uncertainties of the charged and neutral species exists. The measured $R_{\text{out}}/R_{\text{side}}$ ratios are slightly larger for kaons than for pions. This is an indication of different space-time correlations for pions and kaons, and a more prolonged emission duration for kaons.

In our previous pion femtoscopy analysis [9] the information about the emission time (decoupling time) at

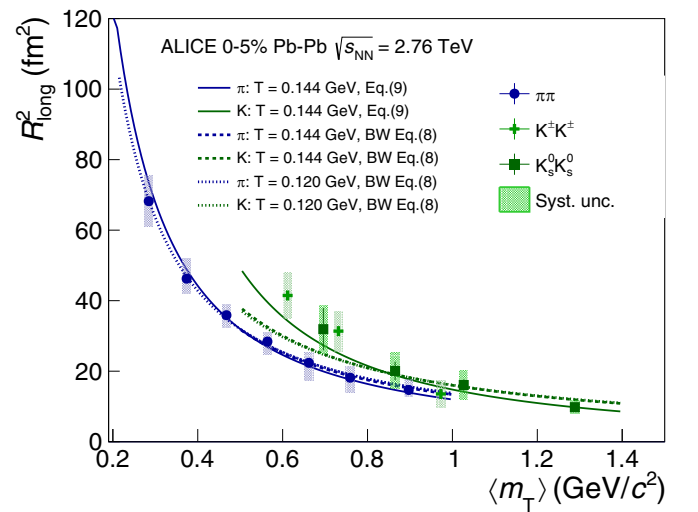


FIG. 8. R_{long}^2 vs m_T for kaons and pions. The solid lines show the fit using Eq. (9) for pions and kaons to extract the emission times (τ); the dashed and dotted lines show the fit using Eq. (8) with $T_{\text{kin}} = 0.144$ GeV and $T_{\text{kin}} = 0.120$ GeV, respectively. For pions at small m_T , the dashed and dotted line coincide.

TABLE IV. Emission times for pions and kaons extracted using the blast-wave (BW) formula (8) and the analytical formula (9).

Method	T (GeV)	α_π	α_K	τ_π (fm/c)	τ_K (fm/c)
Fit with BW Eq. (8)	0.120			9.6 ± 0.2	10.6 ± 0.1
Fit with BW Eq. (8)	0.144			8.8 ± 0.2	9.5 ± 0.1
Fit with Eq. (9)	0.144	5.0	2.2	9.3 ± 0.2	11.0 ± 0.1
Fit with Eq. (9)	0.144	4.3 ± 2.3	1.6 ± 0.7	9.5 ± 0.2	11.6 ± 0.1

kinetic freeze-out $\tau \sim 10$ fm/c was extracted by fitting the m_T dependence of R_{long}^2 by using the blast-wave expression [58]

$$R_{\text{long}}^2 = \tau^2 \frac{T_{\text{kin}}}{m_T} \frac{K_2(m_T)}{K_1(m_T)}, \quad (8)$$

where T_{kin} is the temperature at kinetic freeze-out, and K_n are the integer-order modified Bessel functions. We tried to use Eq. (8) to fit the $R_{\text{long}}^2 m_T$ dependence (Fig. 8) for pions and kaons by taking the thermal freeze-out temperature $T_{\text{kin}} = 0.120$ GeV as in Ref. [9] (dotted lines) and $T_{\text{kin}} = 0.144$ GeV (dashed lines). The emission times extracted from the fit are presented in Table IV. However, although this formula works well for pions, it fails to describe kaon longitudinal radii. Large transverse flow may be partially responsible for this failure [34]. The following analytical formula for the time of maximal emission, τ_{max} , is proposed in Ref. [34]:

$$R_{\text{long}}^2 = \tau_{\text{max}}^2 \frac{T_{\text{max}}}{m_T \cosh y_T} \left(1 + \frac{3T_{\text{max}}}{2m_T \cosh y_T} \right), \quad (9)$$

where $\cosh y_T = (1 - v_T^2)^{-1/2}$, $v_T = \frac{\beta p_T}{\beta m_T + \alpha}$, T_{max} is the temperature at the hypersurface of maximal emission, $\beta = 1/T_{\text{max}}$, and α is a free parameter determining the intensity of flow.² The advantage of Eq. (9) is that it is derived for a scenario with transverse flow of any intensity, which is especially important for LHC energies.

The analytical formula (9) was used to fit the m_T dependence of R_{long}^2 (Fig. 8). The fit was performed by using the following parameters determined in Ref. [34] by fitting light flavor particle spectra [59]: $T_{\text{max}} = 0.144$ GeV, and $\alpha_\pi = 5.0$ and $\alpha_K = 2.2$.

The extracted times of maximal emission are presented in Table IV.

²The authors of Ref. [34] use full evolutionary model (HKM) that has no sharp or sudden kinetic freeze-out. For such type of models a continuous hadron emission takes place instead. Then for each particle species, considered within certain transverse momentum bin, there is a four-dimensional (4D) layer, adjacent to the spacelike hypersurface of maximal emission, from where most of the selected particles are emitted. This nonenclosed hypersurface is characterized by the (average) proper time τ_{max} —time of maximal emission, and the effective temperature T_{max} . The proposed phenomenological expression for R_{long} is associated just with this hypersurface and is based on the model that is different from the blast-wave parametrization for sudden freeze-out. So the blast-wave temperature T_{kin} can differ from the temperature parameter T_{max} .

To estimate the systematic errors of the extracted times of maximal emission we also have performed fitting with T_{max} , α_π , and α_K varied within the range of their uncertainty [34]: ± 0.03 GeV, ± 3.5 , and ± 0.7 , respectively. The maximum deviations from the central values appeared to be $(+1.8, -0.5)$ fm/c for pions and $(+0.5, -0.1)$ fm/c for kaons. These systematic errors are fully correlated. Regardless of the specific parameter choice, we consistently observe the time of maximal emission for kaons to be larger than the one for pions. The extracted times of maximal emission are rather close to those obtained within the HKM model [34]: $\tau_\pi = 9.44 \pm 0.02$ fm/c, $\tau_K = 12.40 \pm 0.04$ fm/c.³ There is evidence that the time of maximal emission for pions is smaller than the one for kaons. This observation can explain the observed breaking of m_T scaling between pions and kaons. It is interesting to note that in Ref. [34] this difference in the emission times is explained by the different influence of resonances on pions and kaons during the rescattering phase due to kaon rescattering through the $K^*(892)$ resonance (with lifetime of 4–5 fm/c). It was shown in Ref. [34] that a significant regeneration of the $K^*(892)$ takes place in full HKM simulations with rescatterings (UrQMD cascade), whereas this process is not present in a scenario where only resonance decays are taken into account.

Similar findings were reported in Ref. [60], where the production yield of $K^*(892)$ in heavy-ion collisions at the LHC was studied. Also there, the inclusion of a hadronic phase in the theoretical modeling of the production process proved to be essential in order to reproduce the experimentally found suppression pattern of $K^*(892)$ production when compared with pp collisions [61].

V. SUMMARY

We presented the first results of three-dimensional femtoscopic analyses for charged and neutral kaons in Pb-Pb collisions at $\sqrt{s_{NN}} = 2.76$ TeV.

³These results were obtained in Ref. [34] by using the small interval $q = 0-0.04$ GeV/c in order to minimize influence of the non-Gaussian tails. It is found in Ref. [34] that, if even strong non-Gaussian behavior is observed for the kaon correlation function in a wide q interval, one can nevertheless utilize the same formula (9), but making the parameter α free for kaons. Then one gets practically the same effective time for kaon emission, as is obtained from the fit of the correlation function in the small interval $q = 0-0.04$ GeV/c; for pions there is no such problem.

A decrease of source radii with increasing transverse mass and decreasing event multiplicity was observed. The m_T scaling expected by pure hydrodynamical models appears to be broken in our data. A scaling of pion and kaon radii with k_T was observed instead. The measured ratio of transverse radii $R_{\text{out}}/R_{\text{side}}$ is larger for kaons than for pions, indicating different space-time correlations. A new approach [34] for extracting the emission times for pions and especially for kaons was applied. It was shown that the measured time of maximal emission for kaons is larger than that of pions.

The comparison of measured three-dimensional radii with a model, wherein the hydrodynamic phase is followed by the hadronic rescattering phase [33], and pure hydrodynamical calculations [32,33] has shown that pion femtoscopic radii are well reproduced by both approaches while the behavior of the three-dimensional kaon radii can be described only if the hadronic rescattering phase is present in the model.

ACKNOWLEDGMENTS

The ALICE Collaboration would like to thank all its engineers and technicians for their invaluable contributions to the construction of the experiment and the CERN accelerator teams for the outstanding performance of the LHC complex. The ALICE Collaboration gratefully acknowledges the resources and support provided by all Grid centers and the Worldwide LHC Computing Grid (WLCG) Collaboration. The ALICE Collaboration acknowledges the following funding agencies for their support in building and running the ALICE detector: A. I. Alikhanyan National Science Laboratory (Yerevan Physics Institute) Foundation (ANSL), State Committee of Science and World Federation of Scientists (WFS), Armenia; Austrian Academy of Sciences and Nationalstiftung für Forschung, Technologie und Entwicklung, Austria; Ministry of Communications and High Technologies, National Nuclear Research Center, Azerbaijan; Conselho Nacional de Desenvolvimento Científico e Tecnológico (CNPq), Universidade Federal do Rio Grande do Sul (UFRGS), Financiadora de Estudos e Projetos (Finep) and Fundação de Amparo à Pesquisa do Estado de São Paulo (FAPESP), Brazil; Ministry of Science & Technology of China (MSTC), National Natural Science Foundation of China (NSFC) and Ministry of Education of China (MOEC), China; Ministry of Science, Education and Sport and Croatian Science Foundation, Croatia; Ministry of Education, Youth and Sports of the Czech Republic, Czech Republic; The Danish Council for Independent Research | Natural Sciences, the Carlsberg Foundation and Danish National Research Foundation (DNRF), Denmark; Helsinki Institute of Physics (HIP), Finland; Commissariat à l’Energie Atomique (CEA) and Institut National de Physique Nucléaire et de Physique des Particules (IN2P3) and Cen-

tre National de la Recherche Scientifique (CNRS), France; Bundesministerium für Bildung, Wissenschaft, Forschung und Technologie (BMBF) and GSI Helmholtzzentrum für Schwerionenforschung GmbH, Germany; General Secretariat for Research and Technology, Ministry of Education, Research and Religions, Greece; National Research, Development and Innovation Office, Hungary; Department of Atomic Energy Government of India (DAE) and Council of Scientific and Industrial Research (CSIR), New Delhi, India; Indonesian Institute of Science, Indonesia; Centro Fermi–Museo Storico della Fisica e Centro Studi e Ricerche Enrico Fermi and Istituto Nazionale di Fisica Nucleare (INFN), Italy; Institute for Innovative Science and Technology, Nagasaki Institute of Applied Science (IIST), Japan Society for the Promotion of Science (JSPS) KAKENHI and Japanese Ministry of Education, Culture, Sports, Science and Technology (MEXT), Japan; Consejo Nacional de Ciencia (CONACYT) y Tecnología, through Fondo de Cooperación Internacional en Ciencia y Tecnología (FONCICYT) and Dirección General de Asuntos del Personal Académico (DGAPA), Mexico; Nederlandse Organisatie voor Wetenschappelijk Onderzoek (NWO), Netherlands; The Research Council of Norway, Norway; Commission on Science and Technology for Sustainable Development in the South (COMSATS), Pakistan; Pontificia Universidad Católica del Perú, Peru; Ministry of Science and Higher Education and National Science Centre, Poland; Korea Institute of Science and Technology Information and National Research Foundation of Korea (NRF), Republic of Korea; Ministry of Education and Scientific Research, Institute of Atomic Physics and Romanian National Agency for Science, Technology and Innovation, Romania; Joint Institute for Nuclear Research (JINR), Ministry of Education and Science of the Russian Federation and National Research Centre Kurchatov Institute, Russia; Ministry of Education, Science, Research and Sport of the Slovak Republic, Slovakia; National Research Foundation of South Africa, South Africa; Centro de Aplicaciones Tecnológicas y Desarrollo Nuclear (CEADEN), Cubaenergía, Cuba, Ministerio de Ciencia e Innovación and Centro de Investigaciones Energéticas, Medioambientales y Tecnológicas (CIEMAT), Spain; Swedish Research Council (VR) and Knut & Alice Wallenberg Foundation (KAW), Sweden; European Organization for Nuclear Research, Switzerland; National Science and Technology Development Agency (NSDTA), Suranaree University of Technology (SUT) and Office of the Higher Education Commission under NRU project of Thailand, Thailand; Turkish Atomic Energy Agency (TAEK), Turkey; National Academy of Sciences of Ukraine, Ukraine; Science and Technology Facilities Council (STFC), United Kingdom; National Science Foundation of the United States of America (NSF) and United States Department of Energy, Office of Nuclear Physics (DOE NP), United States of America.

- [1] N. Cabibbo and G. Parisi, Exponential hadronic spectrum and quark liberation, *Phys. Lett. B* **59**, 67 (1975).
 [2] E. V. Shuryak, Quantum chromodynamics and the theory of superdense matter, *Phys. Rep.* **61**, 71 (1980).

- [3] J. Adams *et al.* (STAR Collaboration), Experimental and theoretical challenges in the search for the quark gluon plasma: The STAR Collaboration’s critical assessment of the evidence from RHIC collisions, *Nucl. Phys. A* **757**, 102 (2005).

- [4] B. B. Back *et al.* (PHOBOS Collaboration), The PHOBOS perspective on discoveries at RHIC, *Nucl. Phys. A* **757**, 28 (2005).
- [5] K. Adcox *et al.* (PHENIX Collaboration), Formation of dense partonic matter in relativistic nucleus-nucleus collisions at RHIC: Experimental evaluation by the PHENIX collaboration, *Nucl. Phys. A* **757**, 184 (2005).
- [6] K. Aamodt *et al.* (ALICE Collaboration), Elliptic Flow of Charged Particles in Pb-Pb Collisions at $\sqrt{s_{NN}} = 2.76$ TeV, *Phys. Rev. Lett.* **105**, 252302 (2010).
- [7] B. B. Abelev *et al.* (ALICE Collaboration), Elliptic flow of identified hadrons in Pb-Pb collisions at $\sqrt{s_{NN}} = 2.76$ TeV, *J. High Energy Phys.* **06** (2015) 190.
- [8] J. Adam *et al.* (ALICE Collaboration), Measurement of jet suppression in central Pb-Pb collisions at $\sqrt{s_{NN}} = 2.76$ TeV, *Phys. Lett. B* **746**, 1 (2015).
- [9] K. Aamodt *et al.* (ALICE Collaboration), Two-pion Bose-Einstein correlations in central Pb-Pb collisions at $\sqrt{s_{NN}} = 2.76$ TeV, *Phys. Lett. B* **696**, 328 (2011).
- [10] G. Goldhaber, S. Goldhaber, W.-Y. Lee, and A. Pais, Influence of Bose-Einstein statistics on the antiproton-proton annihilation process, *Phys. Rev.* **120**, 300 (1960).
- [11] G. Kopylov and M. Podgoretsky, Correlations of identical particles emitted by highly excited nuclei, *Sov. J. Nucl. Phys.* **15**, 219 (1972).
- [12] G. Kopylov, V. Lyuboshits, and M. Podgoretsky, Correlations between the particles which have small relative momenta, JINR-P2-8069 (1974).
- [13] R. Lednicky, Correlation femtoscopy, *Nucl. Phys. A* **774**, 189 (2006).
- [14] M. A. Lisa, S. Pratt, R. Soltz, and U. Wiedemann, Femtoscopy in relativistic heavy ion collisions, *Annu. Rev. Nucl. Part. Sci.* **55**, 357 (2005).
- [15] Yu. M. Sinyukov, S. V. Akkelin, I. A. Karpenko, and Y. Hama, Kinetics versus hydrodynamics: Generalization of Landau/Cooper-Frye prescription for freeze-out, *Acta Phys. Polon., B* **40**, 1025 (2009).
- [16] W. Broniowski, M. Chojnacki, W. Florkowski, and A. Kisiel, Uniform Description of Soft Observables in Heavy-Ion Collisions at $\sqrt{s_{NN}} = 200$ GeV, *Phys. Rev. Lett.* **101**, 022301 (2008).
- [17] J. Vredevoogd and S. Pratt, Universal Flow in the First fm/c at RHIC, *Nucl. Phys. A* **830**, 515C (2009).
- [18] K. Aamodt *et al.* (ALICE Collaboration), The ALICE experiment at the CERN LHC, *J. Instrum.* **3**, S08002 (2008).
- [19] J. Adam *et al.* (ALICE Collaboration), Centrality dependence of pion freeze-out radii in Pb-Pb collisions at $\sqrt{s_{NN}} = 2.76$ TeV, *Phys. Rev. C* **93**, 024905 (2016).
- [20] I. G. Bearden *et al.* (NA44 Collaboration), Space-time evolution of the hadronic source in peripheral to central Pb + Pb collisions, *Eur. Phys. J. C* **18**, 317 (2000).
- [21] A. N. Makhlin and Y. M. Sinyukov, The hydrodynamics of hadron matter under a pion interferometric microscope, *Z. Phys. C: Part. Fields* **39**, 69 (1988).
- [22] I. G. Bearden *et al.* (NA44 Collaboration), Two-Kaon Correlations in Central Pb + Pb Collisions at 158A GeV/c, *Phys. Rev. Lett.* **87**, 112301 (2001).
- [23] S. V. Afanasiev *et al.* (NA49 Collaboration), Bose-Einstein correlations of charged kaons in central Pb + Pb collisions at $E_{\text{beam}} = 158$ GeV per nucleon, *Phys. Lett. B* **557**, 157 (2003).
- [24] J. Adams *et al.* (STAR Collaboration), Identified Particle Distributions in pp and Au + Au Collisions at $\sqrt{s_{NN}} = 200$ GeV, *Phys. Rev. Lett.* **92**, 112301 (2004).
- [25] L. Adamczyk *et al.* (STAR Collaboration), Freeze-out dynamics via charged kaon femtoscopy in $\sqrt{s_{NN}} = 200$ GeV central Au + Au collisions, *Phys. Rev. C* **88**, 034906 (2013).
- [26] B. I. Abelev *et al.* (STAR Collaboration), Neutral kaon interferometry in Au + Au collisions at $\sqrt{s_{NN}} = 200$ GeV, *Phys. Rev. C* **74**, 054902 (2006).
- [27] S. Afanasiev *et al.* (PHENIX Collaboration), Kaon interferometric probes of space-time evolution in Au + Au collisions at $\sqrt{s_{NN}} = 200$ GeV, *Phys. Rev. Lett.* **103**, 142301 (2009).
- [28] A. Adare *et al.* (PHENIX Collaboration), Systematic study of charged-pion and kaon femtoscopy in Au + Au collisions at $\sqrt{s_{NN}} = 200$ GeV, *Phys. Rev. C* **92**, 034914 (2015).
- [29] I. A. Karpenko, Yu. M. Sinyukov, and K. Werner, Uniform description of bulk observables in the hydrokinetic model of A + A collisions at the BNL Relativistic Heavy Ion Collider and the CERN Large Hadron Collider, *Phys. Rev. C* **87**, 024914 (2013).
- [30] I. A. Karpenko and Yu. M. Sinyukov, Kaon and pion femtoscopy at the highest energies available at the BNL Relativistic Heavy Ion Collider (RHIC) in a hydrokinetic model, *Phys. Rev. C* **81**, 054903 (2010).
- [31] J. Adam *et al.* (ALICE Collaboration), One-dimensional pion, kaon, and proton femtoscopy in Pb-Pb collisions at $\sqrt{s_{NN}} = 2.76$ TeV, *Phys. Rev. C* **92**, 054908 (2015).
- [32] A. Kisiel, M. Galazyn, and P. Bozek, Pion, kaon, and proton femtoscopy in Pb-Pb collisions at $\sqrt{s_{NN}} = 2.76$ TeV modeled in (3 + 1)D hydrodynamics, *Phys. Rev. C* **90**, 064914 (2014).
- [33] V. M. Shapoval, P. Braun-Munzinger, I. A. Karpenko, and Yu. M. Sinyukov, Femtoscopy correlations of kaons in Pb + Pb collisions at LHC within hydrokinetic model, *Nucl. Phys. A* **929**, 1 (2014).
- [34] Yu. M. Sinyukov, V. M. Shapoval, and V. Yu. Naboka, On m_T dependence of femtoscopy scales for meson and baryon pairs, *Nucl. Phys. A* **946**, 227 (2016).
- [35] A. Kisiel, W. Broniowski, M. Chojnacki, and W. Florkowski, Azimuthally sensitive femtoscopy in hydrodynamics with statistical hadronization from the BNL Relativistic Heavy Ion Collider to the CERN Large Hadron Collider, *Phys. Rev. C* **79**, 014902 (2009).
- [36] I. A. Karpenko and Yu. M. Sinyukov, Energy dependence of pion interferometry scales in ultra-relativistic heavy ion collisions, *Phys. Lett. B* **688**, 50 (2010).
- [37] B. Abelev *et al.* (ALICE Collaboration), Centrality determination of Pb-Pb collisions at $\sqrt{s_{NN}} = 2.76$ TeV with ALICE, *Phys. Rev. C* **88**, 044909 (2013).
- [38] G. Dellacasa *et al.* (ALICE Collaboration), *ALICE: Technical Design Report of the Time Projection Chamber*, CERN, Geneva (2000).
- [39] P. Cortese *et al.* (ALICE Collaboration), *ALICE Time-of-Flight System (TOF): Addendum to the Technical Design Report*, Technical Design Report ALICE; CERN, Geneva (2002); <https://cds.cern.ch/record/545834>.
- [40] B. B. Abelev *et al.* (ALICE Collaboration), Performance of the ALICE experiment at the CERN LHC, *Int. J. Mod. Phys. A* **29**, 1430044 (2014).
- [41] X.-N. Wang and M. Gyulassy, HIJING: A Monte Carlo model for multiple jet production in pp, pA and AA collisions, *Phys. Rev. D* **44**, 3501 (1991).

- [42] R. Brun, F. Bruyant, F. Carminati, S. Giani, M. Maire, A. McPherson, G. Patrick, and L. Urban, *GEANT Detector Description and Simulation Tool*, Geneva (1994), Long Writeup W5013.
- [43] K. A. Olive *et al.* (Particle Data Group Collaboration), Review of particle physics, *Chin. Phys. C* **38**, 090001 (2014).
- [44] M. Steinpreis, Neutral Kaon Femtoscopy in Pb-Pb Collisions at $\sqrt{s_{NN}} = 2.76$ TeV at the LHC with ALICE, Ph.D. thesis, Ohio State University, 2014 (unpublished).
- [45] B. Abelev *et al.* (ALICE Collaboration), $K_s^0 - K_s^0$ correlations in pp collisions at $\sqrt{s} = 7$ TeV from the LHC ALICE experiment, *Phys. Lett. B* **717**, 151 (2012).
- [46] M. G. Bowler, Coulomb corrections to Bose-Einstein correlations have been greatly exaggerated, *Phys. Lett. B* **270**, 69 (1991).
- [47] Yu. Sinyukov, R. Lednicky, S. V. Akkelin, J. Pluta, and B. Erazmus, Coulomb corrections for interferometry analysis of expanding hadron systems, *Phys. Lett. B* **432**, 248 (1998).
- [48] S. V. Akkelin, R. Lednicky, and Yu. M. Sinyukov, Correlation search for coherent pion emission in heavy ion collisions, *Phys. Rev. C* **65**, 064904 (2002).
- [49] B. B. Abelev *et al.* (ALICE Collaboration), Two- and three-pion quantum statistics correlations in Pb-Pb collisions at $\sqrt{s_{NN}} = 2.76$ TeV at the CERN Large Hadron Collider, *Phys. Rev. C* **89**, 024911 (2014).
- [50] U. A. Wiedemann and U. W. Heinz, Resonance contributions to Hanbury-Brown-Twiss correlation radii, *Phys. Rev. C* **56**, 3265 (1997).
- [51] R. Lednicky and V. L. Lyuboshits, Final state interaction effect on pairing correlations between particles with small relative momenta, *Sov. J. Nucl. Phys.* **35**, 770 (1982) [*Yad. Fiz.* **35**, 1316 (1981)].
- [52] A. Antonelli, Radiative phi decays, eConf **C020620**, 65 (2002).
- [53] N. N. Achasov and V. V. Gubin, Analysis of the nature of the $\phi \rightarrow \gamma\pi\eta$ and $\phi \rightarrow \gamma\pi^0\pi^0$ decays, *Phys. Atom. Nucl.* **65**, 1528 (2002); *Phys. Rev. D* **63**, 094007 (2001).
- [54] N. N. Achasov and A. V. Kiselev, The new analysis of the KLOE data on the $\phi \rightarrow \eta\pi^0\gamma$ decay, *Phys. Rev. D* **68**, 014006 (2003).
- [55] A. D. Martin, E. N. Ozmumlu, and E. J. Squires, The $\pi\pi$ and $K\bar{K}$ amplitudes, the S^* and the quark structure of 0^{++} resonances, *Nucl. Phys. B* **121**, 514 (1977).
- [56] S. E. Koonin, Proton pictures of high-energy nuclear collisions, *Phys. Lett. B* **70**, 43 (1977).
- [57] S. Pratt, T. Csorgo, and J. Zimanyi, Detailed predictions for two-pion correlations in ultrarelativistic heavy ion collisions, *Phys. Rev. C* **42**, 2646 (1990).
- [58] M. Herrmann and G. F. Bertsch, Source dimensions in ultrarelativistic heavy-ion collisions, *Phys. Rev. C* **51**, 328 (1995).
- [59] B. Abelev *et al.* (ALICE Collaboration), Centrality dependence of π , K, p production in Pb-Pb collisions at $\sqrt{s_{NN}} = 2.76$ TeV, *Phys. Rev. C* **88**, 044910 (2013).
- [60] A. G. Knospe, C. Markert, K. Werner, J. Steinheimer, and M. Bleicher, Hadronic resonance production and interaction in partonic and hadronic matter in the EPOS3 model with and without the hadronic afterburner UrQMD, *Phys. Rev. C* **93**, 014911 (2016).
- [61] K. Aamodt *et al.* (ALICE Collaboration), Centrality Dependence of the Charged-Particle Multiplicity Density at Midrapidity in Pb-Pb Collisions at $\sqrt{s_{NN}} = 2.76$ TeV, *Phys. Rev. Lett.* **106**, 032301 (2011).

S. Acharya,¹³⁹ J. Adam,⁹⁹ D. Adamová,⁹⁶ J. Adolfsson,³⁴ M. M. Aggarwal,¹⁰¹ G. Aglieri Rinella,³⁵ M. Agnello,³¹ N. Agrawal,⁴⁸ Z. Ahammed,¹³⁹ N. Ahmad,¹⁷ S. U. Ahn,⁸⁰ S. Aiola,¹⁴³ A. Akindinov,⁶⁵ S. N. Alam,¹³⁹ J. L. B. Alba,¹¹⁴ D. S. D. Albuquerque,¹²⁵ D. Aleksandrov,⁹² B. Alessandro,⁵⁹ R. Alfaro Molina,⁷⁵ A. Alici,^{54,27,12} A. Alkin,³ J. Alme,²² T. Alt,⁷¹ L. Altenkamper,²² I. Altsybeev,¹³⁸ C. Alves Garcia Prado,¹²⁴ C. Andrei,⁸⁹ D. Andreou,³⁵ H. A. Andrews,¹¹³ A. Andronic,¹⁰⁹ V. Anguelov,¹⁰⁶ C. Anson,⁹⁹ T. Antičić,¹¹⁰ F. Antinori,⁵⁷ P. Antonioli,⁵⁴ R. Anwar,¹²⁷ L. Aphecetche,¹¹⁷ H. Appelshäuser,⁷¹ S. Arcelli,²⁷ R. Arnaldi,⁵⁹ O. W. Arnold,^{107,36} I. C. Arsene,²¹ M. Arslandok,¹⁰⁶ B. Audurier,¹¹⁷ A. Augustinus,³⁵ R. Auerbeck,¹⁰⁹ M. D. Azmi,¹⁷ A. Badalà,⁵⁶ Y. W. Baek,^{61,79} S. Bagnasco,⁵⁹ R. Bailhache,⁷¹ R. Bala,¹⁰³ A. Baldissieri,⁷⁶ M. Ball,⁴⁵ R. C. Baral,⁶⁸ A. M. Barbano,²⁶ R. Barbera,²⁸ F. Barile,^{33,53} L. Barioglio,²⁶ G. G. Barnaföldi,¹⁴² L. S. Barnby,⁹⁵ V. Barret,⁸² P. Bartalini,⁷ K. Barth,³⁵ E. Bartsch,⁷¹ M. Basile,²⁷ N. Bastid,⁸² S. Basu,¹⁴¹ G. Batigne,¹¹⁷ B. Batyunya,⁷⁸ P. C. Batzing,²¹ I. G. Bearden,⁹³ H. Beck,¹⁰⁶ C. Bedda,⁶⁴ N. K. Behera,⁶¹ I. Belikov,¹³⁵ F. Bellini,^{27,35} H. Bello Martinez,² R. Bellwied,¹²⁷ L. G. E. Beltran,¹²³ V. Belyaev,⁸⁵ G. Bencedi,¹⁴² S. Beole,²⁶ A. Bercuci,⁸⁹ Y. Berdnikov,⁹⁸ D. Berenyi,¹⁴² R. A. Bertens,¹³⁰ D. Berzano,³⁵ L. Betev,³⁵ A. Bhasin,¹⁰³ I. R. Bhat,¹⁰³ A. K. Bhati,¹⁰¹ B. Bhattacharjee,⁴⁴ J. Bhom,¹²¹ L. Bianchi,¹²⁷ N. Bianchi,⁵¹ C. Bianchin,¹⁴¹ J. Bielčik,³⁹ J. Bielčíková,⁹⁶ A. Bilandzic,^{107,36} G. Biro,¹⁴² R. Biswas,⁴ S. Biswas,⁴ J. T. Blair,¹²² D. Blau,⁹² C. Blume,⁷¹ G. Boca,¹³⁶ F. Bock,^{84,35,106} A. Bogdanov,⁸⁵ L. Boldizsár,¹⁴² M. Bombara,⁴⁰ G. Bonomi,¹³⁷ M. Bonora,³⁵ J. Book,⁷¹ H. Borel,⁷⁶ A. Borissov,¹⁹ M. Borri,¹²⁹ E. Botta,²⁶ C. Bourjau,⁹³ L. Bratrud,⁷¹ P. Braun-Munzinger,¹⁰⁹ M. Bregant,¹²⁴ T. A. Broker,⁷¹ M. Broz,³⁹ E. J. Brucken,⁴⁶ E. Bruna,⁵⁹ G. E. Bruno,³³ D. Budnikov,¹¹¹ H. Buesching,⁷¹ S. Bufalino,³¹ P. Buhler,¹¹⁶ P. Buncic,³⁵ O. Busch,¹³³ Z. Buthelezi,⁷⁷ J. B. Butt,¹⁵ J. T. Buxton,¹⁸ J. Cabala,¹¹⁹ D. Caffarri,^{35,94} H. Caines,¹⁴³ A. Caliva,⁶⁴ E. Calvo Villar,¹¹⁴ P. Camerini,²⁵ A. A. Capon,¹¹⁶ F. Carena,³⁵ W. Carena,³⁵ F. Carnesecchi,^{27,12} J. Castillo Castellanos,⁷⁶ A. J. Castro,¹³⁰ E. A. R. Casula,⁵⁵ C. Ceballos Sanchez,⁹ P. Cerello,⁵⁹ S. Chandra,¹³⁹ B. Chang,¹²⁸ S. Chapeland,³⁵ M. Chartier,¹²⁹ S. Chattopadhyay,¹³⁹ S. Chattopadhyay,¹¹² A. Chauvin,^{36,107} M. Cherney,⁹⁹ C. Cheshkov,¹³⁴ B. Cheynis,¹³⁴ V. Chibante Barroso,³⁵ D. D. Chinellato,¹²⁵ S. Cho,⁶¹ P. Chochula,³⁵ M. Chojnacki,⁹³ S. Choudhury,¹³⁹ T. Chowdhury,⁸² P. Christakoglou,⁹⁴ C. H. Christensen,⁹³ P. Christiansen,³⁴ T. Chujo,¹³³ S. U. Chung,¹⁹ C. Cicalo,⁵⁵ L. Cifarelli,^{12,27} F. Cindolo,⁵⁴ J. Cleymans,¹⁰² F. Colamaria,³³ D. Colella,^{35,66} A. Collu,⁸⁴

- M. Colocci,²⁷ M. Concas,^{59,a} G. Conesa Balbastre,⁸³ Z. Conesa del Valle,⁶² M. E. Connors,^{143,b} J. G. Contreras,³⁹ T. M. Cormier,⁹⁷ Y. Corrales Morales,⁵⁹ I. Cortés Maldonado,² P. Cortese,³² M. R. Cosentino,¹²⁶ F. Costa,³⁵ S. Costanza,¹³⁶ J. Crkovská,⁶² P. Crochet,⁸² E. Cuautle,⁷³ L. Cunqueiro,⁷² T. Dahms,^{36,107} A. Dainese,⁵⁷ M. C. Danisch,¹⁰⁶ A. Danu,⁶⁹ D. Das,¹¹² I. Das,¹¹² S. Das,⁴ A. Dash,⁹⁰ S. Dash,⁴⁸ S. De,^{124,49} A. De Caro,³⁰ G. de Cataldo,⁵³ C. de Conti,¹²⁴ J. de Cuveland,⁴² A. De Falco,²⁴ D. De Gruttola,^{30,12} N. De Marco,⁵⁹ S. De Pasquale,³⁰ R. D. De Souza,¹²⁵ H. F. Degenhardt,¹²⁴ A. Deisting,^{109,106} A. Deloff,⁸⁸ C. Deplano,⁹⁴ P. Dhankeher,⁴⁸ D. Di Bari,³³ A. Di Mauro,³⁵ P. Di Nezza,⁵¹ B. Di Ruzza,⁵⁷ M. A. Diaz Corchero,¹⁰ T. Dietel,¹⁰² P. Dillenseger,⁷¹ R. Divià,³⁵ Ø. Djuvsland,²² A. Dobrin,³⁵ D. Domenicis Gimenez,¹²⁴ B. Dönigus,⁷¹ O. Dordic,²¹ L. V. V. Doremalen,⁶⁴ A. K. Dubey,¹³⁹ A. Dubla,¹⁰⁹ L. Ducroux,¹³⁴ A. K. Duggal,¹⁰¹ P. Dupieux,⁸² R. J. Ehlers,¹⁴³ D. Elia,⁵³ E. Endress,¹¹⁴ H. Engel,⁷⁰ E. Epple,¹⁴³ B. Erasmus,¹¹⁷ F. Erhardt,¹⁰⁰ B. Espagnon,⁶² S. Esumi,¹³³ G. Eulisse,³⁵ J. Eum,¹⁹ D. Evans,¹¹³ S. Evdokimov,¹¹⁵ L. Fabbietti,^{107,36} J. Faivre,⁸³ A. Fantoni,⁵¹ M. Fasel,^{97,84} L. Feldkamp,⁷² A. Feliciello,⁵⁹ G. Feofilov,¹³⁸ J. Ferencei,⁹⁶ A. Fernández Téllez,² E. G. Ferreira,¹⁶ A. Ferretti,²⁶ A. Festanti,^{29,35} V. J. G. Feuillard,^{76,82} J. Figiel,¹²¹ M. A. S. Figueredo,¹²⁴ S. Filchagin,¹¹¹ D. Finogeev,⁶³ F. M. Fionda,^{22,24} E. M. Fiore,³³ M. Floris,³⁵ S. Foertsch,⁷⁷ P. Foka,¹⁰⁹ S. Fokin,⁹² E. Fragiaco,⁶⁰ A. Francescon,³⁵ A. Francisco,¹¹⁷ U. Frankenfeld,¹⁰⁹ G. G. Fronze,²⁶ U. Fuchs,³⁵ C. Furget,⁸³ A. Furs,⁶³ M. Fusco Girard,³⁰ J. J. Gaardhøje,⁹³ M. Gagliardi,²⁶ A. M. Gago,¹¹⁴ K. Gajdosova,⁹³ M. Gallio,²⁶ C. D. Galvan,¹²³ P. Ganoti,⁸⁷ C. Garabatos,¹⁰⁹ E. Garcia-Solis,¹³ K. Garg,²⁸ C. Gargiulo,³⁵ P. Gasik,^{36,107} E. F. Gauger,¹²² M. B. Gay Ducati,⁷⁴ M. Germain,¹¹⁷ J. Ghosh,¹¹² P. Ghosh,¹³⁹ S. K. Ghosh,⁴ P. Gianotti,⁵¹ P. Giubellino,^{109,59,35} P. Giubilato,²⁹ E. Gladysz-Dziadus,¹²¹ P. Glässel,¹⁰⁶ D. M. Gómez Coral,⁷⁵ A. Gomez Ramirez,⁷⁰ A. S. Gonzalez,³⁵ V. Gonzalez,¹⁰ P. González-Zamora,¹⁰ S. Gorbunov,⁴² L. Görlich,¹²¹ S. Gotovac,¹²⁰ V. Grabski,⁷⁵ L. K. Graczykowski,¹⁴⁰ K. L. Graham,¹¹³ L. Greiner,⁸⁴ A. Grelli,⁶⁴ C. Grigoras,³⁵ V. Grigoriev,⁸⁵ A. Grigoryan,¹ S. Grigoryan,⁷⁸ N. Grion,⁶⁰ J. M. Gronefeld,¹⁰⁹ F. Grosa,³¹ J. F. Grosse-Oetringhaus,³⁵ R. Grosso,¹⁰⁹ L. Gruber,¹¹⁶ F. Guber,⁶³ R. Guernane,⁸³ B. Guerzoni,²⁷ K. Gulbrandsen,⁹³ T. Gunji,¹³² A. Gupta,¹⁰³ R. Gupta,¹⁰³ I. B. Guzman,² R. Haake,³⁵ C. Hadjidakis,⁶² H. Hamagaki,⁸⁶ G. Hamar,¹⁴² J. C. Hamon,¹³⁵ M. R. Haque,⁶⁴ J. W. Harris,¹⁴³ A. Harton,¹³ H. Hassan,⁸³ D. Hatzifotiadou,^{12,54} S. Hayashi,¹³² S. T. Heckel,⁷¹ E. Hellbär,⁷¹ H. Helstrup,³⁷ A. Hergelegiu,⁸⁹ G. Herrera Corral,¹¹ F. Herrmann,⁷² B. A. Hess,¹⁰⁵ K. F. Hetland,³⁷ H. Hillemanns,³⁵ C. Hills,¹²⁹ B. Hippolyte,¹³⁵ J. Hladky,⁶⁷ B. Hohlweger,¹⁰⁷ D. Horak,³⁹ S. Hornung,¹⁰⁹ R. Hosokawa,^{133,83} P. Hristov,³⁵ C. Hughes,¹³⁰ T. J. Humanic,¹⁸ N. Hussain,⁴⁴ T. Hussain,¹⁷ D. Hutter,⁴² D. S. Hwang,²⁰ S. A. Iga Buitron,⁷³ R. Ilkaev,¹¹¹ M. Inaba,¹³³ M. Ippolitov,^{85,92} M. Irfan,¹⁷ M. S. Islam,¹¹² M. Ivanov,¹⁰⁹ V. Ivanov,⁹⁸ V. Izucheev,¹¹⁵ B. Jacak,⁸⁴ N. Jacazio,²⁷ P. M. Jacobs,⁸⁴ M. B. Jadhav,⁴⁸ J. Jadlovsky,¹¹⁹ S. Jaelani,⁶⁴ C. Jahnke,³⁶ M. J. Jakubowska,¹⁴⁰ M. A. Janik,¹⁴⁰ P. H. S. Y. Jayarathna,¹²⁷ C. Jena,⁹⁰ S. Jena,¹²⁷ M. Jercic,¹⁰⁰ R. T. Jimenez Bustamante,¹⁰⁹ P. G. Jones,¹¹³ A. Jusko,¹¹³ P. Kalinak,⁶⁶ A. Kalweit,³⁵ J. H. Kang,¹⁴⁴ V. Kaplin,⁸⁵ S. Kar,¹³⁹ A. Karasu Uysal,⁸¹ O. Karavichev,⁶³ T. Karavicheva,⁶³ L. Karayan,^{109,106} P. Karczmarczyk,³⁵ E. Karpechev,⁶³ U. Kebschull,⁷⁰ R. Keidel,¹⁴⁵ D. L. D. Keijdener,⁶⁴ M. Keil,³⁵ B. Ketzer,⁴⁵ Z. Khabanova,⁹⁴ P. Khan,¹¹² S. A. Khan,¹³⁹ A. Khanzadeev,⁹⁸ Y. Kharlov,¹¹⁵ A. Khatun,¹⁷ A. Khuntia,⁴⁹ M. M. Kielbowicz,¹²¹ B. Kileng,³⁷ B. Kim,¹³³ D. Kim,¹⁴⁴ D. J. Kim,¹²⁸ H. Kim,¹⁴⁴ J. S. Kim,⁴³ J. Kim,¹⁰⁶ M. Kim,⁶¹ M. Kim,¹⁴⁴ S. Kim,²⁰ T. Kim,¹⁴⁴ S. Kirsch,⁴² I. Kisel,⁴² S. Kiselev,⁶⁵ A. Kisiel,¹⁴⁰ G. Kiss,¹⁴² J. L. Klay,⁶ C. Klein,⁷¹ J. Klein,³⁵ C. Klein-Bösing,⁷² S. Klewin,¹⁰⁶ A. Kluge,³⁵ M. L. Knichel,^{35,106} A. G. Knospe,¹²⁷ C. Kobdaj,¹¹⁸ M. Kofarago,¹⁴² T. Kollegger,¹⁰⁹ V. Kondratiev,¹³⁸ N. Kondratyeva,⁸⁵ E. Kondratyuk,¹¹⁵ A. Konevskikh,⁶³ M. Konyushikhin,¹⁴¹ M. Kopcik,¹¹⁹ M. Kour,¹⁰³ C. Kouzinopoulos,³⁵ O. Kovalenko,⁸⁸ V. Kovalenko,¹³⁸ M. Kowalski,¹²¹ G. Koyithatta Meethalevedu,⁴⁸ I. Králik,⁶⁶ A. Kravčáková,⁴⁰ M. Krivda,^{66,113} F. Krizek,⁹⁶ E. Kryshen,⁹⁸ M. Krzewicki,⁴² A. M. Kubera,¹⁸ V. Kučera,⁹⁶ C. Kuhn,¹³⁵ P. G. Kuijser,⁹⁴ A. Kumar,¹⁰³ J. Kumar,⁴⁸ L. Kumar,¹⁰¹ S. Kumar,⁴⁸ S. Kundu,⁹⁰ P. Kurashvili,⁸⁸ A. Kurepin,⁶³ A. B. Kurepin,⁶³ A. Kuryakin,¹¹¹ S. Kushpil,⁹⁶ M. J. Kweon,⁶¹ Y. Kwon,¹⁴⁴ S. L. La Pointe,⁴² P. La Rocca,²⁸ C. Lagana Fernandes,¹²⁴ Y. S. Lai,⁸⁴ I. Lakomov,³⁵ R. Langoy,⁴¹ K. Lapidus,¹⁴³ C. Lara,⁷⁰ A. Lardeux,^{21,76} A. Lattuca,²⁶ E. Laudi,³⁵ R. Lavicka,³⁹ R. Lea,²⁵ L. Leardini,¹⁰⁶ S. Lee,¹⁴⁴ F. Lehas,⁹⁴ S. Lehner,¹¹⁶ J. Lehrbach,⁴² R. C. Lemmon,⁹⁵ V. Lenti,⁵³ E. Leogrande,⁶⁴ I. León Monzón,¹²³ P. Lévai,¹⁴² X. Li,¹⁴ J. Lien,⁴¹ R. Lietava,¹¹³ B. Lim,¹⁹ S. Lindal,²¹ V. Lindenstruth,⁴² S. W. Lindsay,¹²⁹ C. Lippmann,¹⁰⁹ M. A. Lisa,¹⁸ V. Litichevskiy,⁴⁶ W. J. Llope,¹⁴¹ D. F. Lodato,⁶⁴ P. I. Loenne,²² V. Loginov,⁸⁵ C. Loizides,⁸⁴ P. Loncar,¹²⁰ X. Lopez,⁸² E. López Torres,⁹ A. Lowe,¹⁴² P. Luettig,⁷¹ J. R. Luhder,⁷² M. Lunardon,²⁹ G. Luparello,^{60,25} M. Lupi,³⁵ T. H. Lutz,¹⁴³ A. Maevskaya,⁶³ M. Mager,³⁵ S. Mahajan,¹⁰³ S. M. Mahmood,²¹ A. Maire,¹³⁵ R. D. Majka,¹⁴³ M. Malaev,⁹⁸ L. Malinina,^{78,c} D. Mal'Kevich,⁶⁵ P. Malzacher,¹⁰⁹ A. Mamonov,¹¹¹ V. Manko,⁹² F. Manso,⁸² V. Manzari,⁵³ Y. Mao,⁷ M. Marchisone,^{77,131} J. Mareš,⁶⁷ G. V. Margagliotti,²⁵ A. Margotti,⁵⁴ J. Margutti,⁶⁴ A. Marín,¹⁰⁹ C. Markert,¹²² M. Marquard,⁷¹ N. A. Martin,¹⁰⁹ P. Martinengo,³⁵ J. A. L. Martinez,⁷⁰ M. I. Martínez,² G. Martínez García,¹¹⁷ M. Martínez Pedreira,³⁵ A. Mas,¹²⁴ S. Masciocchi,¹⁰⁹ M. Masera,²⁶ A. Masoni,⁵⁵ E. Masson,¹¹⁷ A. Mastroserio,⁵³ A. M. Mathis,^{107,36} A. Matyja,^{121,130} C. Mayer,¹²¹ J. Mazer,¹³⁰ M. Mazzilli,³³ M. A. Mazzoni,⁵⁸ F. Meddi,²³ Y. Melikyan,⁸⁵ A. Menchaca-Rocha,⁷⁵ E. Meninno,³⁰ J. Mercado Pérez,¹⁰⁶ M. Meres,³⁸ S. Mhlanga,¹⁰² Y. Miao,¹³³ M. M. Mieskolainen,⁴⁶ D. L. Mihaylov,¹⁰⁷ K. Mikhaylov,^{65,78} J. Milosevic,²¹ A. Mischke,⁶⁴ A. N. Mishra,⁴⁹ D. Miśkowiec,¹⁰⁹ J. Mitra,¹³⁹ C. M. Mitu,⁶⁹ N. Mohammadi,⁶⁴ B. Mohanty,⁹⁰ M. Mohisin Khan,^{17,d} E. Montes,¹⁰ D. A. Moreira De Godoy,⁷² L. A. P. Moreno,² S. Moretto,²⁹ A. Morreale,¹¹⁷ A. Morsch,³⁵ V. Muccifora,⁵¹ E. Mudnic,¹²⁰ D. Mühlheim,⁷² S. Muhuri,¹³⁹ M. Mukherjee,⁴ J. D. Mulligan,¹⁴³ M. G. Munhoz,¹²⁴ K. Mürning,⁴⁵ R. H. Munzer,⁷¹ H. Murakami,¹³² S. Murray,⁷⁷ L. Musa,³⁵ J. Musinsky,⁶⁶ C. J. Myers,¹²⁷ J. W. Myrcha,¹⁴⁰ D. Nag,⁴ B. Naik,⁴⁸ R. Nair,⁸⁸ B. K. Nandi,⁴⁸ R. Nania,^{12,54} E. Nappi,⁵³ A. Narayan,⁴⁸ M. U. Naru,¹⁵ H. Natal da Luz,¹²⁴ C. Nattrass,¹³⁰ S. R. Navarro,² K. Nayak,⁹⁰ R. Nayak,⁴⁸ T. K. Nayak,¹³⁹ S. Nazarenko,¹¹¹ A. Nedosekin,⁶⁵ R. A. Negrao De Oliveira,³⁵

L. Nellen,⁷³ S. V. Nesbo,³⁷ F. Ng,¹²⁷ M. Nicassio,¹⁰⁹ M. Niculescu,⁶⁹ J. Niedziela,^{35,140} B. S. Nielsen,⁹³ S. Nikolaev,⁹² S. Nikulin,⁹² V. Nikulin,⁹⁸ F. Noferini,^{54,12} P. Nomokonov,⁷⁸ G. Nooren,⁶⁴ J. C. C. Noris,² J. Norman,¹²⁹ A. Nyanin,⁹² J. Nystrand,²² H. Oeschler,^{106,e} S. Oh,¹⁴³ A. Ohlson,^{35,106} T. Okubo,⁴⁷ L. Olah,¹⁴² J. Oleniacz,¹⁴⁰ A. C. Oliveira Da Silva,¹²⁴ M. H. Oliver,¹⁴³ J. Onderwaater,¹⁰⁹ C. Oppedisano,⁵⁹ R. Orava,⁴⁶ M. Oravec,¹¹⁹ A. Ortiz Velasquez,⁷³ A. Oskarsson,³⁴ J. Otwinowski,¹²¹ K. Oyama,⁸⁶ Y. Pachmayer,¹⁰⁶ V. Pacik,⁹³ D. Pagano,¹³⁷ P. Pagano,³⁰ G. Pačić,⁷³ P. Palni,⁷ J. Pan,¹⁴¹ A. K. Pandey,⁴⁸ S. Panebianco,⁷⁶ V. Papikyan,¹ G. S. Pappalardo,⁵⁶ P. Pareek,⁴⁹ J. Park,⁶¹ S. Parmar,¹⁰¹ A. Passfeld,⁷² S. P. Pathak,¹²⁷ V. Paticchio,⁵³ R. N. Patra,¹³⁹ B. Paul,⁵⁹ H. Pei,⁷ T. Peitzmann,⁶⁴ X. Peng,⁷ L. G. Pereira,⁷⁴ H. Pereira Da Costa,⁷⁶ D. Peresunko,^{92,85} E. Perez Lezama,⁷¹ V. Peskov,⁷¹ Y. Pestov,⁵ V. Petráček,³⁹ V. Petrov,¹¹⁵ M. Petrovici,⁸⁹ C. Petta,²⁸ R. P. Pezzi,⁷⁴ S. Piano,⁶⁰ M. Pikaň,³⁸ P. Pillot,¹¹⁷ L. O. D. L. Pimentel,⁹³ O. Pinazza,^{35,54} L. Pinsky,¹²⁷ D. B. Piyarathna,¹²⁷ M. Płoskoń,⁸⁴ M. Planinic,¹⁰⁰ F. Pliquett,⁷¹ J. Pluta,¹⁴⁰ S. Pochybova,¹⁴² P. L. M. Podesta-Lerma,¹²³ M. G. Poghosyan,⁹⁷ B. Polichtchouk,¹¹⁵ N. Poljak,¹⁰⁰ W. Poonsawat,¹¹⁸ A. Pop,⁸⁹ H. Poppenborg,⁷² S. Porteboeuf-Houssais,⁸² V. Pozdniakov,⁷⁸ S. K. Prasad,⁴ R. Preghenella,⁵⁴ F. Prino,⁵⁹ C. A. Pruneau,¹⁴¹ I. Pshenichnov,⁶³ M. Puccio,²⁶ G. Puddu,²⁴ P. Pujahari,¹⁴¹ V. Punin,¹¹¹ J. Putschke,¹⁴¹ A. Rachevski,⁶⁰ S. Raha,⁴ S. Rajput,¹⁰³ J. Rak,¹²⁸ A. Rakotozafindrabe,⁷⁶ L. Ramello,³² F. Rami,¹³⁵ D. B. Rana,¹²⁷ R. Raniwala,¹⁰⁴ S. Raniwala,¹⁰⁴ S. S. Räsänen,⁴⁶ B. T. Rascanu,⁷¹ D. Rathee,¹⁰¹ V. Ratza,⁴⁵ I. Ravasenga,³¹ K. F. Read,^{97,130} K. Redlich,^{88,f} A. Rehman,²² P. Reichelt,⁷¹ F. Reidt,³⁵ X. Ren,⁷ R. Renfordt,⁷¹ A. R. Reolon,⁵¹ A. Reshetin,⁶³ K. Reygers,¹⁰⁶ V. Riabov,⁹⁸ R. A. Ricci,⁵² T. Richert,⁶⁴ M. Richter,²¹ P. Riedler,³⁵ W. Riegler,³⁵ F. Riggi,²⁸ C. Ristea,⁶⁹ M. Rodríguez Cahuantzi,² K. Røed,²¹ E. Rogochaya,⁷⁸ D. Rohr,^{42,35} D. Röhrich,²² P. S. Rokita,¹⁴⁰ F. Ronchetti,⁵¹ E. D. Rosas,⁷³ P. Rosnet,⁸² A. Rossi,^{29,57} A. Rotondi,¹³⁶ F. Roukoutakis,⁸⁷ A. Roy,⁴⁹ C. Roy,¹³⁵ P. Roy,¹¹² A. J. Rubio Montero,¹⁰ O. V. Rueda,⁷³ R. Rui,²⁵ B. Rumyantsev,⁷⁸ A. Rustamov,⁹¹ E. Ryabinkin,⁹² Y. Ryabov,⁹⁸ A. Rybicki,¹²¹ S. Saarinén,⁴⁶ S. Sadhu,¹³⁹ S. Sadovskiy,¹¹⁵ K. Šafařík,³⁵ S. K. Saha,¹³⁹ B. Sahlmuller,⁷¹ B. Sahoo,⁴⁸ P. Sahoo,⁴⁹ R. Sahoo,⁴⁹ S. Sahoo,⁶⁸ P. K. Sahu,⁶⁸ J. Saini,¹³⁹ S. Sakai,¹³³ M. A. Saleh,¹⁴¹ J. Salzwedel,¹⁸ S. Sambyal,¹⁰³ V. Samsonov,^{85,98} A. Sandoval,⁷⁵ D. Sarkar,¹³⁹ N. Sarkar,¹³⁹ P. Sarma,⁴⁴ M. H. P. Sas,⁶⁴ E. Scapparone,⁵⁴ F. Scarlassara,²⁹ R. P. Scharenberg,¹⁰⁸ H. S. Scheid,⁷¹ C. Schiaua,⁸⁹ R. Schicker,¹⁰⁶ C. Schmidt,¹⁰⁹ H. R. Schmidt,¹⁰⁵ M. O. Schmidt,¹⁰⁶ M. Schmidt,¹⁰⁵ N. V. Schmidt,^{71,97} S. Schuchmann,¹⁰⁶ J. Schukraft,³⁵ Y. Schutz,^{135,117,35} K. Schwarz,¹⁰⁹ K. Schweda,¹⁰⁹ G. Scioli,²⁷ E. Scomparin,⁵⁹ R. Scott,¹³⁰ M. Šefčík,⁴⁰ J. E. Seger,⁹⁹ Y. Sekiguchi,¹³² D. Sekihata,⁴⁷ I. Selyuzhenko,^{85,109} K. Senosi,⁷⁷ S. Senyukov,^{35,3,135} E. Serradilla,^{10,75} P. Sett,⁴⁸ A. Sevcenco,⁶⁹ A. Shabanov,⁶³ A. Shabetai,¹¹⁷ R. Shahoyan,³⁵ W. Shaikh,¹¹² A. Shagaraev,¹¹⁵ A. Sharma,¹⁰¹ A. Sharma,¹⁰³ M. Sharma,¹⁰³ N. Sharma,¹⁰³ N. Sharma,^{101,130} A. I. Sheikh,¹³⁹ K. Shigaki,⁴⁷ Q. Shou,⁷ K. Shtejer,^{9,26} Y. Sibiriyak,⁹² S. Siddhanta,⁵⁵ K. M. Sielewicz,³⁵ T. Siemiarczuk,⁸⁸ D. Silvermyr,³⁴ C. Silvestre,⁸³ G. Simatovic,¹⁰⁰ G. Simonetti,³⁵ R. Singaraju,¹³⁹ R. Singh,⁹⁰ V. Singhal,¹³⁹ T. Sinha,¹¹² B. Sitar,³⁸ M. Sitta,³² T. B. Skaali,²¹ M. Slupecki,¹²⁸ N. Smirnov,¹⁴³ R. J. M. Snellings,⁶⁴ T. W. Snellman,¹²⁸ J. Song,¹⁹ M. Song,¹⁴⁴ F. Soramel,²⁹ S. Sorensen,¹³⁰ F. Sozzi,¹⁰⁹ E. Spiriti,⁵¹ I. Sputowska,¹²¹ B. K. Srivastava,¹⁰⁸ J. Stachel,¹⁰⁶ I. Stan,⁶⁹ P. Stankus,⁹⁷ E. Stenlund,³⁴ D. Stocco,¹¹⁷ M. M. Storetvedt,³⁷ P. Strmen,³⁸ A. A. P. Suaide,¹²⁴ T. Sugitate,⁴⁷ C. Suire,⁶² M. Suleymanov,¹⁵ M. Suljic,²⁵ R. Sultanov,⁶⁵ M. Šumbera,⁹⁶ S. Sumowidagdo,⁵⁰ K. Suzuki,¹¹⁶ S. Swain,⁶⁸ A. Szabo,³⁸ I. Szarka,³⁸ U. Tabassam,¹⁵ J. Takahashi,¹²⁵ G. J. Tambave,²² N. Tanaka,¹³³ M. Tarhini,⁶² M. Tariq,¹⁷ M. G. Tarzila,⁸⁹ A. Tauro,³⁵ G. Tejada Muñoz,² A. Telesca,³⁵ K. Terasaki,¹³² C. Terrevoli,²⁹ B. Teyssier,¹³⁴ D. Thakur,⁴⁹ S. Thakur,¹³⁹ D. Thomas,¹²² F. Thoresen,⁹³ R. Tieulent,¹³⁴ A. Tikhonov,⁶³ A. R. Timmins,¹²⁷ A. Toia,⁷¹ S. R. Torres,¹²³ S. Tripathy,⁴⁹ S. Trogolo,²⁶ G. Trombetta,³³ L. Tropp,⁴⁰ V. Trubnikov,³ W. H. Trzaska,¹²⁸ B. A. Trzeciak,⁶⁴ T. Tsuji,¹³² A. Tumkin,¹¹¹ R. Turrisi,⁵⁷ T. S. Tveter,²¹ K. Ullaland,²² E. N. Umaka,¹²⁷ A. Uras,¹³⁴ G. L. Usai,²⁴ A. Utrobicic,¹⁰⁰ M. Vala,^{119,66} J. Van Der Maarel,⁶⁴ J. W. Van Hoorne,³⁵ M. van Leeuwen,⁶⁴ T. Vanat,⁹⁶ P. Vande Vyvre,³⁵ D. Varga,¹⁴² A. Vargas,² M. Vargyas,¹²⁸ R. Varma,⁴⁸ M. Vasileiou,⁸⁷ A. Vasiliev,⁹² A. Vauthier,⁸³ O. Vázquez Doce,^{107,36} V. Vechernin,¹³⁸ A. M. Veen,⁶⁴ A. Velure,²² E. Vercellin,²⁶ S. Vergara Limón,² R. Vernet,⁸ R. Vértesi,¹⁴² L. Vickovic,¹²⁰ S. Vigolo,⁶⁴ J. Viinikainen,¹²⁸ Z. Vilakazi,¹³¹ O. Villalobos Baillie,¹¹³ A. Villatoro Tello,² A. Vinogradov,⁹² L. Vinogradov,¹³⁸ T. Virgili,³⁰ V. Vislavicius,³⁴ A. Vodopyanov,⁷⁸ M. A. Völkl,^{106,105} K. Voloshin,⁶⁵ S. A. Voloshin,¹⁴¹ G. Volpe,³³ B. von Haller,³⁵ I. Vorobyev,^{107,36} D. Voscek,¹¹⁹ D. Vranic,^{35,109} J. Vrláková,⁴⁰ B. Wagner,²² H. Wang,⁶⁴ M. Wang,⁷ D. Watanabe,¹³³ Y. Watanabe,^{132,133} M. Weber,¹¹⁶ S. G. Weber,¹⁰⁹ D. F. Weiser,¹⁰⁶ S. C. Wenzel,³⁵ J. P. Wessels,⁷² U. Westerhoff,⁷² A. M. Whitehead,¹⁰² J. Wiechula,⁷¹ J. Wikne,²¹ G. Wilk,⁸⁸ J. Wilkinson,^{106,54} G. A. Willems,⁷² M. C. S. Williams,⁵⁴ E. Willsher,¹¹³ B. Windelband,¹⁰⁶ W. E. Witt,¹³⁰ S. Yalcin,⁸¹ K. Yamakawa,⁴⁷ P. Yang,⁷ S. Yano,⁴⁷ Z. Yin,⁷ H. Yokoyama,^{133,83} I.-K. Yoo,^{35,19} J. H. Yoon,⁶¹ V. Yurchenko,³ V. Zaccolo,^{59,93} A. Zaman,¹⁵ C. Zampolli,³⁵ H. J. C. Zanoli,¹²⁴ N. Zardoshti,¹¹³ A. Zarochentsev,¹³⁸ P. Závada,⁶⁷ N. Zaviyalov,¹¹¹ H. Zbroszczyk,¹⁴⁰ M. Zhalov,⁹⁸ H. Zhang,^{22,7} X. Zhang,⁷ Y. Zhang,⁷ C. Zhang,⁶⁴ Z. Zhang,^{82,7} C. Zhao,²¹ N. Zhigareva,⁶⁵ D. Zhou,⁷ Y. Zhou,⁹³ Z. Zhou,²² H. Zhu,²² J. Zhu,⁷ A. Zichichi,^{12,27} A. Zimmermann,¹⁰⁶ M. B. Zimmermann,³⁵ G. Zinovjev,³ J. Zmeskal,¹¹⁶ and S. Zou⁷

(ALICE Collaboration)

¹A.I. Alikhanyan National Science Laboratory (Yerevan Physics Institute) Foundation, Yerevan, Armenia²Benemérita Universidad Autónoma de Puebla, Puebla, Mexico³Bogolyubov Institute for Theoretical Physics, Kiev, Ukraine⁴Bose Institute, Department of Physics and Centre for Astroparticle Physics and Space Science (CAPSS), Kolkata, India⁵Budker Institute for Nuclear Physics, Novosibirsk, Russia

- ⁶California Polytechnic State University, San Luis Obispo, California, United States
- ⁷Central China Normal University, Wuhan, China
- ⁸Centre de Calcul de l'IN2P3, Villeurbanne, Lyon, France
- ⁹Centro de Aplicaciones Tecnológicas y Desarrollo Nuclear (CEADEN), Havana, Cuba
- ¹⁰Centro de Investigaciones Energéticas Medioambientales y Tecnológicas (CIEMAT), Madrid, Spain
- ¹¹Centro de Investigación y de Estudios Avanzados (CINVESTAV), Mexico City and Mérida, Mexico
- ¹²Centro Fermi - Museo Storico della Fisica e Centro Studi e Ricerche "Enrico Fermi", Rome, Italy
- ¹³Chicago State University, Chicago, Illinois, United States
- ¹⁴China Institute of Atomic Energy, Beijing, China
- ¹⁵COMSATS Institute of Information Technology (CIIT), Islamabad, Pakistan
- ¹⁶Departamento de Física de Partículas and IGFAE, Universidad de Santiago de Compostela, Santiago de Compostela, Spain
- ¹⁷Department of Physics, Aligarh Muslim University, Aligarh, India
- ¹⁸Department of Physics, Ohio State University, Columbus, Ohio, United States
- ¹⁹Department of Physics, Pusan National University, Pusan, Republic of Korea
- ²⁰Department of Physics, Sejong University, Seoul, Republic of Korea
- ²¹Department of Physics, University of Oslo, Oslo, Norway
- ²²Department of Physics and Technology, University of Bergen, Bergen, Norway
- ²³Dipartimento di Fisica dell'Università 'La Sapienza' and Sezione INFN, Rome, Italy
- ²⁴Dipartimento di Fisica dell'Università and Sezione INFN, Cagliari, Italy
- ²⁵Dipartimento di Fisica dell'Università and Sezione INFN, Trieste, Italy
- ²⁶Dipartimento di Fisica dell'Università and Sezione INFN, Turin, Italy
- ²⁷Dipartimento di Fisica e Astronomia dell'Università and Sezione INFN, Bologna, Italy
- ²⁸Dipartimento di Fisica e Astronomia dell'Università and Sezione INFN, Catania, Italy
- ²⁹Dipartimento di Fisica e Astronomia dell'Università and Sezione INFN, Padova, Italy
- ³⁰Dipartimento di Fisica 'E.R. Caianiello' dell'Università and Gruppo Collegato INFN, Salerno, Italy
- ³¹Dipartimento DISAT del Politecnico and Sezione INFN, Turin, Italy
- ³²Dipartimento di Scienze e Innovazione Tecnologica dell'Università del Piemonte Orientale and INFN Sezione di Torino, Alessandria, Italy
- ³³Dipartimento Interateneo di Fisica 'M. Merlin' and Sezione INFN, Bari, Italy
- ³⁴Division of Experimental High Energy Physics, University of Lund, Lund, Sweden
- ³⁵European Organization for Nuclear Research (CERN), Geneva, Switzerland
- ³⁶Excellence Cluster Universe, Technische Universität München, Munich, Germany
- ³⁷Faculty of Engineering, Bergen University College, Bergen, Norway
- ³⁸Faculty of Mathematics, Physics and Informatics, Comenius University, Bratislava, Slovakia
- ³⁹Faculty of Nuclear Sciences and Physical Engineering, Czech Technical University in Prague, Prague, Czech Republic
- ⁴⁰Faculty of Science, P.J. Šafárik University, Košice, Slovakia
- ⁴¹Faculty of Technology, Buskerud and Vestfold University College, Tonsberg, Norway
- ⁴²Frankfurt Institute for Advanced Studies, Johann Wolfgang Goethe-Universität Frankfurt, Frankfurt, Germany
- ⁴³Gangneung-Wonju National University, Gangneung, Republic of Korea
- ⁴⁴Gauhati University, Department of Physics, Guwahati, India
- ⁴⁵Helmholtz-Institut für Strahlen- und Kernphysik, Rheinische Friedrich-Wilhelms-Universität Bonn, Bonn, Germany
- ⁴⁶Helsinki Institute of Physics (HIP), Helsinki, Finland
- ⁴⁷Hiroshima University, Hiroshima, Japan
- ⁴⁸Indian Institute of Technology Bombay (IIT), Mumbai, India
- ⁴⁹Indian Institute of Technology Indore, Indore, India
- ⁵⁰Indonesian Institute of Sciences, Jakarta, Indonesia
- ⁵¹INFN, Laboratori Nazionali di Frascati, Frascati, Italy
- ⁵²INFN, Laboratori Nazionali di Legnaro, Legnaro, Italy
- ⁵³INFN, Sezione di Bari, Bari, Italy
- ⁵⁴INFN, Sezione di Bologna, Bologna, Italy
- ⁵⁵INFN, Sezione di Cagliari, Cagliari, Italy
- ⁵⁶INFN, Sezione di Catania, Catania, Italy
- ⁵⁷INFN, Sezione di Padova, Padova, Italy
- ⁵⁸INFN, Sezione di Roma, Rome, Italy
- ⁵⁹INFN, Sezione di Torino, Turin, Italy
- ⁶⁰INFN, Sezione di Trieste, Trieste, Italy
- ⁶¹Inha University, Incheon, Republic of Korea
- ⁶²Institut de Physique Nucléaire d'Orsay (IPNO), Université Paris-Sud, CNRS-IN2P3, Orsay, France
- ⁶³Institute for Nuclear Research, Academy of Sciences, Moscow, Russia
- ⁶⁴Institute for Subatomic Physics of Utrecht University, Utrecht, Netherlands

- ⁶⁵*Institute for Theoretical and Experimental Physics, Moscow, Russia*
- ⁶⁶*Institute of Experimental Physics, Slovak Academy of Sciences, Košice, Slovakia*
- ⁶⁷*Institute of Physics, Academy of Sciences of the Czech Republic, Prague, Czech Republic*
- ⁶⁸*Institute of Physics, Bhubaneswar, India*
- ⁶⁹*Institute of Space Science (ISS), Bucharest, Romania*
- ⁷⁰*Institut für Informatik, Johann Wolfgang Goethe-Universität Frankfurt, Frankfurt, Germany*
- ⁷¹*Institut für Kernphysik, Johann Wolfgang Goethe-Universität Frankfurt, Frankfurt, Germany*
- ⁷²*Institut für Kernphysik, Westfälische Wilhelms-Universität Münster, Münster, Germany*
- ⁷³*Instituto de Ciencias Nucleares, Universidad Nacional Autónoma de México, Mexico City, Mexico*
- ⁷⁴*Instituto de Física, Universidade Federal do Rio Grande do Sul (UFRGS), Porto Alegre, Brazil*
- ⁷⁵*Instituto de Física, Universidad Nacional Autónoma de México, Mexico City, Mexico*
- ⁷⁶*IRFU, CEA, Université Paris-Saclay, Saclay, France*
- ⁷⁷*iThemba LABS, National Research Foundation, Somerset West, South Africa*
- ⁷⁸*Joint Institute for Nuclear Research (JINR), Dubna, Russia*
- ⁷⁹*Konkuk University, Seoul, Republic of Korea*
- ⁸⁰*Korea Institute of Science and Technology Information, Daejeon, Republic of Korea*
- ⁸¹*KTO Karatay University, Konya, Turkey*
- ⁸²*Laboratoire de Physique Corpusculaire (LPC), Clermont Université, Université Blaise Pascal, CNRS-IN2P3, Clermont-Ferrand, France*
- ⁸³*Laboratoire de Physique Subatomique et de Cosmologie, Université Grenoble-Alpes, CNRS-IN2P3, Grenoble, France*
- ⁸⁴*Lawrence Berkeley National Laboratory, Berkeley, California, United States*
- ⁸⁵*Moscow Engineering Physics Institute, Moscow, Russia*
- ⁸⁶*Nagasaki Institute of Applied Science, Nagasaki, Japan*
- ⁸⁷*National and Kapodistrian University of Athens, Physics Department, Athens, Greece*
- ⁸⁸*National Centre for Nuclear Studies, Warsaw, Poland*
- ⁸⁹*National Institute for Physics and Nuclear Engineering, Bucharest, Romania*
- ⁹⁰*National Institute of Science Education and Research, HBNI, Jatni, India*
- ⁹¹*National Nuclear Research Center, Baku, Azerbaijan*
- ⁹²*National Research Centre Kurchatov Institute, Moscow, Russia*
- ⁹³*Niels Bohr Institute, University of Copenhagen, Copenhagen, Denmark*
- ⁹⁴*Nikhef, Nationaal instituut voor subatomaire fysica, Amsterdam, Netherlands*
- ⁹⁵*Nuclear Physics Group, STFC Daresbury Laboratory, Daresbury, United Kingdom*
- ⁹⁶*Nuclear Physics Institute, Academy of Sciences of the Czech Republic, Řež u Prahy, Czech Republic*
- ⁹⁷*Oak Ridge National Laboratory, Oak Ridge, Tennessee, United States*
- ⁹⁸*Petersburg Nuclear Physics Institute, Gatchina, Russia*
- ⁹⁹*Physics Department, Creighton University, Omaha, Nebraska, United States*
- ¹⁰⁰*Physics department, Faculty of science, University of Zagreb, Zagreb, Croatia*
- ¹⁰¹*Physics Department, Panjab University, Chandigarh, India*
- ¹⁰²*Physics Department, University of Cape Town, Cape Town, South Africa*
- ¹⁰³*Physics Department, University of Jammu, Jammu, India*
- ¹⁰⁴*Physics Department, University of Rajasthan, Jaipur, India*
- ¹⁰⁵*Physikalisches Institut, Eberhard Karls Universität Tübingen, Tübingen, Germany*
- ¹⁰⁶*Physikalisches Institut, Ruprecht-Karls-Universität Heidelberg, Heidelberg, Germany*
- ¹⁰⁷*Physik Department, Technische Universität München, Munich, Germany*
- ¹⁰⁸*Purdue University, West Lafayette, Indiana, United States*
- ¹⁰⁹*Research Division and ExtreMe Matter Institute EMMI, GSI Helmholtzzentrum für Schwerionenforschung GmbH, Darmstadt, Germany*
- ¹¹⁰*Rudjer Bošković Institute, Zagreb, Croatia*
- ¹¹¹*Russian Federal Nuclear Center (VNIIEF), Sarov, Russia*
- ¹¹²*Saha Institute of Nuclear Physics, Kolkata, India*
- ¹¹³*School of Physics and Astronomy, University of Birmingham, Birmingham, United Kingdom*
- ¹¹⁴*Sección Física, Departamento de Ciencias, Pontificia Universidad Católica del Perú, Lima, Peru*
- ¹¹⁵*SSC IHEP of NRC Kurchatov institute, Protvino, Russia*
- ¹¹⁶*Stefan Meyer Institut für Subatomare Physik (SMI), Vienna, Austria*
- ¹¹⁷*SUBATECH, IMT Atlantique, Université de Nantes, CNRS-IN2P3, Nantes, France*
- ¹¹⁸*Suranaree University of Technology, Nakhon Ratchasima, Thailand*
- ¹¹⁹*Technical University of Košice, Košice, Slovakia*
- ¹²⁰*Technical University of Split FESB, Split, Croatia*
- ¹²¹*The Henryk Niewodniczanski Institute of Nuclear Physics, Polish Academy of Sciences, Cracow, Poland*
- ¹²²*The University of Texas at Austin, Physics Department, Austin, Texas, United States*
- ¹²³*Universidad Autónoma de Sinaloa, Culiacán, Mexico*

- ¹²⁴*Universidade de São Paulo (USP), São Paulo, Brazil*
¹²⁵*Universidade Estadual de Campinas (UNICAMP), Campinas, Brazil*
¹²⁶*Universidade Federal do ABC, Santo Andre, Brazil*
¹²⁷*University of Houston, Houston, Texas, United States*
¹²⁸*University of Jyväskylä, Jyväskylä, Finland*
¹²⁹*University of Liverpool, Liverpool, United Kingdom*
¹³⁰*University of Tennessee, Knoxville, Tennessee, United States*
¹³¹*University of the Witwatersrand, Johannesburg, South Africa*
¹³²*University of Tokyo, Tokyo, Japan*
¹³³*University of Tsukuba, Tsukuba, Japan*
¹³⁴*Université de Lyon, Université Lyon 1, CNRS/IN2P3, IPN-Lyon, Villeurbanne, Lyon, France*
¹³⁵*Université de Strasbourg, CNRS, IPHC UMR 7178, F-67000 Strasbourg, France, Strasbourg, France*
¹³⁶*Università degli Studi di Pavia, Pavia, Italy*
¹³⁷*Università di Brescia, Brescia, Italy*
¹³⁸*V. Fock Institute for Physics, St. Petersburg State University, St. Petersburg, Russia*
¹³⁹*Variable Energy Cyclotron Centre, Kolkata, India*
¹⁴⁰*Warsaw University of Technology, Warsaw, Poland*
¹⁴¹*Wayne State University, Detroit, Michigan, United States*
¹⁴²*Wigner Research Centre for Physics, Hungarian Academy of Sciences, Budapest, Hungary*
¹⁴³*Yale University, New Haven, Connecticut, United States*
¹⁴⁴*Yonsei University, Seoul, Republic of Korea*
¹⁴⁵*Zentrum für Technologietransfer und Telekommunikation (ZTT), Fachhochschule Worms, Worms, Germany*

^aDipartimento DET del Politecnico di Torino, Turin, Italy.

^bGeorgia State University, Atlanta, Georgia, United States.

^cM.V. Lomonosov Moscow State University, D.V. Skobeltsyn Institute of Nuclear, Physics, Moscow, Russia.

^dDepartment of Applied Physics, Aligarh Muslim University, Aligarh, India.

^eDeceased.

^fInstitute of Theoretical Physics, University of Wrocław, Poland.